Fall 12-14-2017

Sorption of 137Cs onto Weathered Micaceous Minerals from Georgia Kaolin Deposits

Dominique Salome Kwong-Moses
Georgia State University

SORPTION OF ^{137}Cs ONTO WEATHERED MICACEOUS MINERALS FROM GEORGIA KAOLIN DEPOSITS

by

DOMINIQUE KWONG-MOSES

Under the Direction of W. Crawford Elliott, Ph.D

ABSTRACT

This study examined the propensity for a weathered muscovite-rich test material to sorb ^{137}Cs in a dilute NaCl solution (1 mmol/L, pH 5) across a range of added stable Cs and Rb concentrations for 130 days at room temperature. This muscovite test material, slaked from processed kaolin ore, was composed of 76% muscovite, 21% kaolinite and 3% quartz. Sorption experiments in the absence of stable Cs and Rb yielded increasing K_d values (1.49×10^3 mL/g to 1.18×10^4 mL/g) over 130 days for ^{137}Cs sorbed onto muscovite. Sorption experiments with stable Cs and Rb displayed linear decreases in Kd values as functions of the concentrations of stable Cs and Rb. These findings are consistent with a Freundlich isotherm. After 130 days, the addition of NaCl (1 mM and 10 mM) caused the desorption of only a small fraction (0.011% - 1.476%) of the sorbed ^{137}Cs from this muscovite test material. The K_d values calculated after the desorption of ^{137}Cs were still generally large 6.93×10^3 mL/g to 1.40×10^6 mL/g. ^{137}Cs was interpreted to be fixed at high affinity sites within the muscovite. This test material showed promise for being a sorbent for radiocesium contaminated waste solutions.

INDEX WORDS: muscovite, mica, kaolin, radiocesium, ^{137}Cs, sorption, Freundlich isotherm, desorption, fixation, legacy waste.

SORPTION OF ^{137}Cs ONTO WEATHERED MICACEOUS MINERALS FROM GEORGIA KAOLIN DEPOSITS

by

DOMINIQUE KWONG-MOSES

An Honors Thesis Submitted in Supplement to the Requirements for the Degree of

Bachelor of Science

in the College of Arts and Sciences

Georgia State University

2017

SORPTION OF ^{137}Cs ONTO WEATHERED MICACEOUS MINERALS FROM GEORGIA KAOLIN DEPOSITS

by

DOMINIQUE KWONG-MOSES

_____

Honors Thesis Director: W. Crawford Elliott

_____

Honors College Associate Dean: Sarah Cook

Electronic Version Approved:

Honors College

Georgia State University

December 2017

DEDICATION

I dedicate this thesis to all future geochemists who started out in a biochemistry-focused department. To friends in the first floor of the library, who are always there to provide much needed banter, laughter, and distractions. To Kyra and Jackson; thank you for taking care of the best mentor any student could ask for. To my parents, for their support. And to Alex for always encouraging me to be my best.

ACKNOWLEDGEMENTS

I would like to thank my mentor, Dr. Crawford Elliott for always keeping his office door open (both figuratively and literally), and always answering my questions, no matter how big, small, or nebulous.

I would also like to thank Dr. Marion Wampler for all his guidance with laboratory methods and data interpretation, and for always providing the most thorough explanations possible.

I would especially like to thank Dr. Brian Powell and his postdoctoral associate, Dr. Helen Xie, for their advice and guidance with calculations and laboratory methods, and for most graciously hosting us and our samples at Clemson University.

Closer to home, I extend thanks to David Davis, a fellow geosciences undergraduate at GSU, for his help running XRD samples and semi-quantitative analyses. And to Nick Allen, a master's student at GSU, for always being willing to answer my obtuse questions about research, chemistry and writing and the like.

And a special thanks to David Avant, for providing the muscovite sample that made this whole project possible.

Finally, I would like to thank the U.S. Department of Energy for funding the radiochemical laboratory at Clemson University, and the National Science Foundation for providing the grant that allowed Drs. W. Crawford Elliott and Daniel M. Deocampo to purchase Georgia State University's XRD.

TABLE OF CONTENTS

LIST OF TABLES

LIST OF FIGURES

1 INTRODUCTION

1.1 Radiocesium in the Environment

Aqueous solutions of low-level radioactive waste have been found percolating through soils adjacent to sites of nuclear activity. A large constituent of this aqueous radioactive waste is radiocesium, ^{137}Cs. Concern for the fate of ^{137}Cs stems fourfold from its high fission yield, moderately long half-life, high solubility and high biological availability (Evans et al., 1983). Due to its high solubility, ^{137}Cs has a high propensity to traverse groundwater and become mobile in certain regolith environments (Cornell, 1993). Radiocesium has a moderately long half-life (30.17 years), compared to other non-transuranic fission products of ^{235}U.

Measureable concentrations of radiocesium have been introduced into the environment as a direct result of nuclear accidents, nuclear weapons testing, and other nuclear development activities. For example, at the Savannah River Site (Aiken, SC, USA), approximately 1900 curies of ^{137}Cs have been released into the environment, as reported in 1991 (Cummins 1991).

Another locality of high radiocesium contamination is the Fukushima Daiichi reactors (Fukushima Prefecture, Japan). Radiocesium and radioactive iodine were accidentally released from the Fukushima-Daiichi Reactor in 2011 in one of the largest accidental releases of

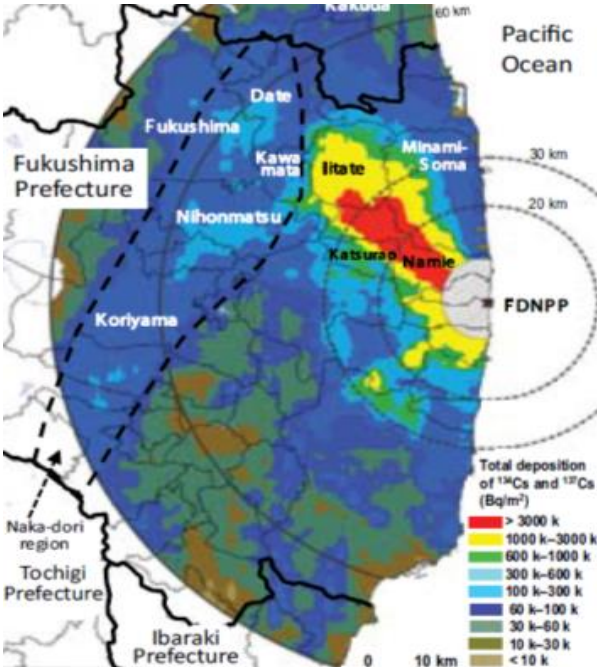

Figure 1 (above): Deposition of ^{134}Cs and ^{137}Cs showing NW movement from the damaged Fukushima Daiichi plant (FDNPP) within the Fukushima Prefecture and neighboring prefectures. Modified from MEXT and DOE data (Yoshida and Takahashi, 2012).

radionuclides. Radioactive iodine decayed within a matter of days; thus, ^{137}Cs is the remaining radionuclide found in soils near Fukushima, Japan. Figure 1 (left) showed the deposition and movement of ^{134}Cs and ^{137}Cs following the accident. Concentrations of radiocesium are listed on the map in units of Bq/m^2.

1.2 Statement of Problem

Micaceous phyllosilicate minerals are known to sorb radiocesium and stable cesium, inferred from studies of soils and from the studies of isolated minerals. The focus of this study is to understand the nature of sorption of radiocesium of a muscovite test material. The muscovite chosen for study is found as gangue material in the Georgia Kaolin deposits (Kogel et. al, 2000). The locality of Georgia kaolin deposits is indicated by the red arrow in the Geological Map of Georgia, USA presented in Figure 2. The Georgia kaolins are located in Sandersville, GA, just south of the Fall Line marking the boundary between the Piedmont (purple) and Coastal Plains (yellow) regions of the state. Georgia's Coastal Plains region developed as a passive continental margin during the Cenozoic Era.

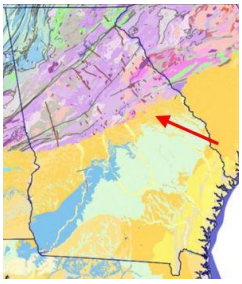

Figure 2 (above): Geological map of GA, USA. Red arrow indicates the locality of muscovite mica sample.

This muscovite has been separated from mined kaolin by Southeast Performance Minerals (David Avant, personal communication, 2017). It is then used in many industrial applications, including paper products, porcelain, concrete and beauty products (Kogel et al., 2000, Prasad et al., 1991). The ability of this muscovite to sorb and fix radiocesium has not been determined. This muscovite test material is predicted to serve as a good sorbent for radiocesium.

1.3 Chemical Nature of Phyllosilicates

Phyllosilicate minerals are layered structures composed of tetrahedral and octahedral coordinated sheets. Muscovite is a 2:1 phyllosilicate mineral composed of two tetrahedral sheets bonded to a dioctahedral sheet, as seen in Figure 3 (left). The layer charge of muscovite is -1. Net layer charge is satisfied by monovalent interlayer cations, most commonly K^+, in the interlayer space between two muscovite layers. The layers themselves are bonded electrostatically while covalent bonds connect Al or Si to ^-OH and O^{2-} respectively. In nature, muscovite weathers in nature first by losing interlayer ions. The loss of interlayer K^+ produces a frayed edge site (FES) (e.g, Figure 4, Wampler et al., 2012). Cesium and/or other alkali metals are easily bonded in frayed edge sites (e.g. Evans et. al, 1983; Lee et. al, 2017).

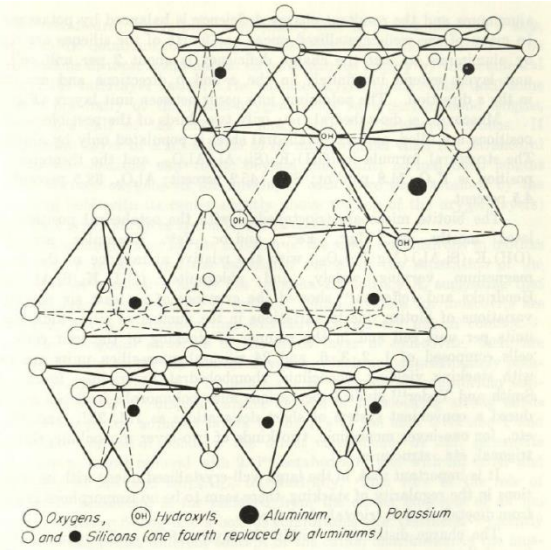

Figure 3 (above): Diagrammatic sketch of the structure of muscovite (Grim 1968), showing tetrahedral and octahedral layers, as well as interlayer cations.

1.4 Radiocesium Sorption by Phyllosilicate Minerals

Through exploitation of the high cation exchange capacity (CEC) of micaceous minerals (vermiculite, illite, and weathered muscovite) for radiocesium, there is potential for in-situ "self-remediation" where these micaceous minerals are present. The radiocesium may be fixed over time to frayed edge sites and/or interlayer zones of

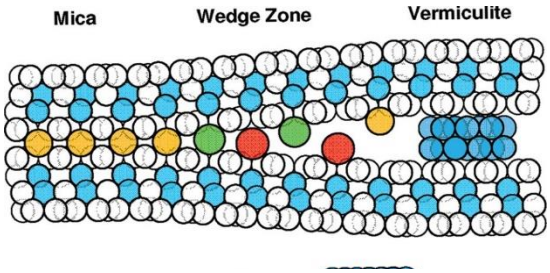

Figure 4 (above): A conceptual model (developed by Wampler et al., 2012) of the cross-section of an interlayer wedge of weathered muscovite mica being transformed to vermiculite. This model illustrates the difference between the exchangeable and fixed Rb and Cs cations in weathered micaceous phases.

weathered mica grains (Goto et al., 2014). Radiocesium and stable Cs are sorbed by cation exchange reactions with phyllosilicate minerals such as vermiculite or weathered muscovite (e.g. Goto et al., 2014, Zaunbrecher et al., 2015a, 2015b, Ishikawa et al., 2017, Fuller et al., 2015). The effective fixation of radiocesium onto weathered mica grains will support the use of weathered muscovite for the in-situ fixation of mobile radiocesium in permeable backfill media, and for the cleanup of liquid low-level radioactive waste in on-site industrial applications.

2 MATERIALS & METHODS

2.1 Sample Provenance

The mica sample (~0.2 kg) studied herein was donated to Georgia State University Department of Geosciences by David Avant (Southeastern Performance Minerals, formerly Georgia Industrial Minerals). This mica was slaked from raw kaolin ore. Southeastern Performance Minerals produced annually 58+ tons of muscovite mica for use in various products such as porcelain, construction materials, beauty products and paper products.

2.2 Sample Splitting

Using a Humboldt sample splitter (chutes: 3/8”), the ~0.2 kg sample was split into smaller ~0.012 kg subsamples or splits. Special care was taken to cover workspace with paper surrounding the splitter to recover material spilled during splitting. Six 0.012 kg splits were produced for this study. The remaining unsplit material (0.1 kg) was stored for further use. Several splits were crushed in preparation for chemical and X-ray diffraction analyses. Two of the sample splits were split again into subsamples of 0.006 kg. These subsamples were crushed in a cleaned ball mill with a tungsten carbide ball for 15 minutes.

A ~0.012 kg split was mailed to Activation Laboratories on Ontario, Canada for a major and trace element assay (Section 2.6). Another ~0.012 kg split was mailed to Dr. Brian Powell at Clemson University, for later use in batch sorption and desorption experiments (Sections 2.8 and 2.9, respectively).

2.3 Sample Sieving

To determine particle distribution of the test muscovite, a bulk sample of 0.5 g was sieved using the following U.S. Standard size sieves: No. 10, No. 20, No. 60, and No. 325. The

mass of each portion at each sieve was weighed and analyzed. Percent particle distribution by particle diameter was determined using Equation 1 as follows:

$$Percent\ Distribution = \frac{m_s}{m_t} \times 100\% \quad (1)$$

In Equation 1 (above), the quantity m_s refers to the mass of the sample at sieve size *s*. The quantity m_t refers to the total mass of the bulk sample sieved.

2.4 X-Ray Diffractometry

A random mount of the powdered split was analyzed using a PANalytical X'Pert Pro™® X-ray diffractometer. This powder was scanned using Cu radiation generated at 45 kV and 40 mA with a nickel filter. The samples were scanned at roughly 1º 2θ/minute from 2-60˚2θ, using a ½ inch divergence and receiving slits. An oriented mount of the power was prepared by transferring a small amount of crushed muscovite in a deionized water slurry onto a petrographic slide and allowed to dry. Two oriented mounts were created. One oriented mount was scanned using conditions similar to the analysis of the powdered bulk sample (air dry). The second oriented mount was solvated in ethylene glycol vapor to detect smectite or interstratified phases (Moore & Reynolds 1998).

D-spacing values obtained from X-ray diffractometry were compared against reference d-spacing values for the minerals muscovite (muscovite $2M_1$), kaolinite (kaolinite $1M_d$), and quartz (quartz low) (Jackson 1985; Moore and Reynolds, 1997). D-spacing values were calculated knowing θ for the observed diffracted peaks. Given θ, the d-spacing values were calculated from Bragg's Law (Equation 2, below):

$$n\lambda = 2\ d\ sin\theta \quad (2)$$

In Bragg's Law (above), λ is the wavelength for Cu radiation filtered with Ni, θ is the angle of diffraction, and *n* is the order of diffraction (effectively $n = 1$ for all reflections).

Additionally, semi-quantitative mineralogical analyses of these mounts were performed to determine estimates of the amounts of minerals present in these splits. The PANalytical HighScore software interfaced to the X-ray diffractometer housed in the Department of Geosciences at Georgia State University provided these semi-quantitative mineralogical analyses.

2.5 Strong Acid Extraction with HNO_3

Four 1.00 g (~0.001 kg) subsamples of the original mica sample and four 1.0 grams (~0.001 kg) test portions of the crushed mica were treated for 3 hours with hot (~100 ˚C), strong (65-70% wt/wt) HNO_3 This nitric acid was diluted to a 50% wt/wt for these extractions to approximate the EPA Method 3050B leaching technique. These tubes were shaken every 15 minutes and vented periodically. Two method blanks (no mica, only nitric acid and centrifuge tube) were also included following the same extraction procedures.

The methods of these extractions used in this study approximated the EPA Method 3050B (Environmental Protection Agency, 1996). These extraction methods were also used in the study of the Savannah River Site soils (Zaunbrecher et al, 2015b). This method was intended to remove metal ions complexed/sorbed on the mineral surfaces of these test portions.

Following treatment, the test portions were centrifuged at 2000 RCF for 10 minutes using the floor model Heraerus Centrifuge. The supernatants were transferred to 15 mL PFA vials and evaporated in the HF hood (located in 615 KH). The salts formed by evaporation were redissolved using 5 mL trace metal grade 2% HNO_3. These test solutions were analyzed for K, Rb, and Cs at Clemson University. All sampling methods for these analyses were conducted gravimetrically rather than volumetrically. A 1g portion of each test solution was then diluted further with 9 g of 2% HNO_3 for analysis of K, Cs and Rb via quadrupole inductively coupled plasma mass spectrometry (ICP-MS), conducted at Clemson University's radiochemical laboratory.

The concentration of aqueous M^+ (Cs, Rb) in the test solutions were calculated using Equation 3 (below). Since each 1 g test sample of each test portion was diluted prior to measurement via ICP-MS, the following dilution correction is made for calculating Cs in solution.

$$[Cs]_{acid\ extractable} = [Cs]_{ICP-MS} \times \frac{m_{total,ICP-MS}}{m_{sample\ removed\ for\ ICP-MS}} \quad (3)$$

All ICP-MS measurements were made using Clemson University's Thermo XSeries II quadrupole ICP-MS under the direction of Professor Brian Powell. The remaining solid residues were re-dissolved in 2% HNO_3 and stored for possible later studies.

2.6 Major and Trace Element Analyses by Activation Laboratories, Ltd.

The mass fractions of major, trace, and lanthanide (Package REE-8) elements of the muscovite test material were determined by Activation Laboratories, Ltd. (Ancaster, Ontario, Canada). Test samples of the muscovite (not crushed) were fused in lithium metaborate/tetraborate fusion. The resultant glass was acidified and analyzed by ICP methods.

2.7 Fractions Extractable

Data obtained from the major and trace element analysis (Section 2.6) and the strong acid extraction (Section 2.5) were used to determine the fractions extractable of Cs, Rb and K, according to the equation:

$$F_{M+} = \frac{[M^+]\ acid\ extractable}{[M^+]\ total} \times 100\ \% \quad (4)$$

Where $[M^+]_{acid\ extractable}$ represents the concentration of Cs, Rb or K measured in the acid treated mica via ICP-MS, as described in 3.3.2a. This analysis includes the dilution correction explained in Equation 3. The quantity $[M^+]_{\text{total}}$ represents the concentration of Cs, Rb or K reported by Activation Laboratories, Ltd.

The values used for *[M^+] measured from acid leaching* are reported in Table 3b as the average values of measured Cs, Rb or K in units of ng/g. The values used for *[M+] in the muscovite* are reported in Table 5 as total Cs, Rb or K measured in the muscovite test material in units of µg/g.

2.8 Batch Sorption Experiments

Further chemical investigations were conducted in a batch setup to determine the mica's ability to sorb ^{133}Cs, ^{137}Cs, and Rb. Twenty-two batch sorption test portions were created gravimetrically using micropipettes. Approximately 0.1000 g aliquots of the mica split (not crushed) were mixed with about 8.0000 g de-ionized water, varying concentrations of stable cesium, and a constant concentration of radiocesium (1.0000 g of 10,000 dpm ^{137}Cs stock solution, per test aliquot). Rb was added to batch sorption test portions 8a, 9a, 10a, 8b, 9b and 10b. To hold ionic strength constant, approximately 1.0 g of 0.01 M NaCl was added to each test portion. The following table (Table 1, below) describes the composition of each batch sorption test portion:

Table 1: Gravimetric Descriptions of Batch Sorption Test Portions

Sample ID	Mass of mica added (g)	Mass of 1.0 x 10^5 dpm ^{137}Cs Stock (g)	Mass of 1.00 x 10^{-3} M ^{133}Cs Stock (g)	Mass of 1.00 x 10^{-4} M ^{133}Cs Stock (g)	Mass of 10 mM NaCl (g)	Mass of Water (g)	Total Sample Mass (g)
1a	0.1299	0.99	0	0	0.9067	7.8531	9.7498
2a	0.1015	0.999	0	0.0453	1.0072	7.8783	9.9298
3a	0.0985	1.007	0	0.1046	1.0081	7.8906	10.0103
4a	0.1099	1.006	0	0.4951	1.0096	7.9281	10.4388
5a	0.102	1.008	0.1	0	1.0094	7.8488	9.9662
6a	0.1094	1.008	0.481	0	1.0095	7.8944	10.3929
7a	0.11	1.002	0.99	0	1.0015	7.8386	10.8321
8a	0.16	1.007	0	0.5013	1.0065	7.9229	10.4377
9a	0.0987	1	0.1	0	1.0066	7.8727	9.9793
10a	0.1028	1.006	0.493	0	1.005	7.877	10.381

11a	0.1458	0	0	0	1.0044	7.8679	8.8723
1b	0.1068	1.007	0	0	1.0029	7.8634	9.8733
2b	0.1044	1.002	0	0.051	1.0075	7.8722	9.9327
3b	0.1158	1.009	0	0.1	1.0059	7.8475	9.9624
4b	0.1348	1.018	0	0.5014	1.0069	7.9466	10.4729
5b	0.12	1.011	0.1	0	1.004	7.8978	10.0128
6b	0.101	1.002	0.499	0	1.0078	7.9142	10.423
7b	0.1046	1.012	0.994	0	1.0068	7.8613	10.8741
8b	0.102	1.004	0	0.4782	1.0056	7.8547	10.3425
9b	0.1228	0.992	0.094	0	1.0043	7.8675	9.9578
10b	0.1094	1.006	0.494	0	1.002	7.8357	10.3377
11b	0.1057	0	0	0	1.0031	7.8432	8.8463

All test portions were tumbled mechanically in Powell's laboratory to facilitate reaction. Following 18 hours, 60 days, and 130 days of tumbling, test portions were sampled for analysis via ICP-MS and liquid scintillation counting. Test portions were removed from the sample tumbler, then centrifuged at 8000 RPM for 20 minutes.

Sampling was executed gravimetrically, wherein 1 ml of supernatant was sampled via pipetting (using VWR micropipettes, and approximated density of the supernatant ≈ 1 g/mL) from each test portion. Each 1 mL sample of supernatant was then weighed to the milligram with an analytical balance. For ICP-MS analysis, the 1 g these subsample portions were diluted with 5 g 2% HNO_3. For the first and second samplings using liquid scintillation counting (LSC), 1 g subsample portions were mixed with approximately 15 mL of high sample load Optiphase HiSafe III scintillation cocktail (a proprietary organic mixture, manufactured by PerkinElmer). For the third sampling, 5 ml of high sample load scintillation was used, based on the number of available LSC vials. Additions of liquid scintillation cocktail were not measured gravimetrically. All liquid scintillation counting measurements were made using a Hewlett Packard TriCarb LSC. These procedures adhered to the practices for handling radionuclides at Clemson University and were overseen by Prof. Brian Powell.

At equilibrium, the partitioning of Cs between the aqueous phase and the solid phase (muscovite) is described in terms of K_d, the distribution coefficient (Goto et al., 2008). For the purposes of this study, K_d is defined as concentration of Cs in the solid phase divided by the concentration of Cs in the aqueous phase as shown in Equation 5 below:

$$K_d = \frac{[Cs]_{solid\ phase}}{[Cs]_{aqueous\ phase}} \quad (5)$$

However, because each 1 g sample of each test portion is diluted prior to measurement via ICP-MS, the following dilution correction is made for the quantities "$[Cs]_{solid\ phase}$" and "$[Cs]_{aqueous\ phase}$" used in Equation 5. The concentration of the concentration of Cs in the solid phase and the concentration of Cs in the aqueous phase are given in Equations 6 and 7.

$$[Cs]_{aqueous} = [Cs]_{ICP-MS} \times \frac{m_{total,ICP-MS}}{m_{sample\ removed\ for\ ICP-MS}} \quad (6)$$

Equation 6 (above) details the dilution correction that should be made for $[Cs]_{aqueous}$. The quantity $[Cs]_{ICP\text{-}MS}$ represents the concentration of Cs directly measured by the ICP-MS. This value is multiplied by the ratio of the mass of the sample measured by ICP-MS to the mass of the subsample removed from the batch sorption test portion for sampling via ICP-MS.

$$[Cs]_{solid\ phase} = \frac{[Cs_{aqueous,t=0} - Cs_{aqueous,(t)}] \times m_{sample}}{m_{mica}} \quad (7)$$

Equation 7 (above) details how $[Cs]_{solid\ phase}$ is calculated from the difference between [Cs] in the aqueous phase at the beginning of the sorption experiment (t = 0) and [Cs] in the aqueous phase at the time of sampling (t). This difference is then multiplied by the mass of the test portion, and normalized to the mass of the mica within that test portion:

The above dilution corrections only need to be made for ICP-MS measurements. For liquid scintillation counting measurements, the concentration of ^{137}Cs measured in dpm is not affected by the volume of scintillation cocktail added to the sample.

2.9 Batch Desorption Experiments

Following third final sampling event for batch sorption experiments at 130 days of tumbling, all 22 test portions were centrifuged at 8000 RPM for 20 minutes. The supernatant liquid was decanted and replaced with 10 g 10 mM $NaCl_{(aq)}$ for 11 test portions, and 10 g 1mM $NaCl_{(aq)}$ for the remaining 11 test portions.

With methods identical to batch sorption experimentation, desorption test portions were subjected to tumbling via mechanical tumbler and test portions were sampled after 60 days. A second collection is planned at 130 days. Sampling procedures for obtaining the 1 g subsample were identical to those procedures used to collect the subsamples from the batch sorption experiments.

For the calculation of K_d, the distribution coefficient for portioning of Cs into the aqueous and solid phases, begin with determining the net count rate measured by liquid scintillation counting. Net count rate is described as the difference between the measured count rate and the background count rate:

$$\sum_{CPM} = CPM_{measured} - CPM_{background} \quad (9)$$

Where Σ_{CPM} represents the net count rate in dpm, $CPM_{measured}$ represents the measured count rate and $CPM_{background}$ represents the background count rate. Net count rate is then divided by the mass of the LSC sample extracted from the test portion to obtain the concentration of Cs in the aqueous phase in dpm/g:

$$[Cs]_{aq} = \frac{\Sigma_{CPM}}{m_{LSC}} \quad (10)$$

Where $[Cs]_{aq}$ represents the concentration of cesium in the aqueous phase in units of dpm/g, Σ_{CPM} represents the net count rate in dpm, and m_{LSC} represents the mass of the LSC sample extracted from the test portion in grams.

Then, the activity of the Cs described is found as the product of the total test portion volume and the concentration of Cs in the aqueous phase:

$$\alpha_{Cs} = m_{LSC} \times [Cs]_{aq} \quad (11)$$

Where α_{Cs} represents the activity of cesium in dpm, m_{LSC} represents the mass of the LSC sample extracted from the test portion in grams, and $[Cs]_{aq}$ represents the concentration of cesium in mol/L present in the aqueous phase. The initial activity on the mica in dpm is calculated as the product of the concentration of Cs on the solid phase (dpm/g) and the mass of mica per test portion (g):

$$\alpha_{i,Cs} = m_{mica} \times [Cs]_{solid} \quad (12)$$

Where $\alpha_{i,\,Cs}$ represents the initial activity on the mica in dpm, m_{mica} represents the mass of mica per test portion in grams, and $[Cs]_{solid}$ represents the concentration of cesium on the solid phase in mol/kg. The difference between the initial activity on the mica and the activity of Cs desorbed (dpm) describes the remaining activity on the total mass of mica:

$$\alpha_{mica} = \alpha_{i,Cs} - \alpha_{Cs} \quad (13)$$

Where α_{mica} represents the remaining activity in dpm on the total mass of mica, $\alpha_{i,\,Cs}$ represemts the initial activity on the mica in dpm and α_{Cs} represents the activity of the Cs desorbed in dpm. The remaining activity on the total mass of mica is divided by the mass of mica per test portion yields the concentration of Cs on the mica in dpm/g:

$$[Cs]_{mica} = \frac{\alpha_{mica}}{m_{mica}} \quad (14)$$

Where $[Cs]_{mica}$ represents the concentration of Cs on the mica in units of dpm per gram, α_{mica} represents the remaining activity on the total mass of mica in dpm, and m_{mica} represents the mass of mica per test portion in grams.

Finally, the concentration of Cs on the mica is divided by the concentration of Cs in the aqueous phase yields the K_d value in units of mL/g.

$$K_d = \frac{[Cs]_{mica}}{[Cs]_{aq}} \quad (15)$$

Where K_d is the partitioning coefficient in mL/g, $[Cs]_{mica}$ represents the concentration of Cs on the mica in units of dpm per gram, and $[Cs]_{aq}$ represents the concentration of cesium in the aqueous phase in dpm/mL.

Liquid scintillation counting data is also used to calculate the fraction of Cs desorbed from the mica, as another measure of the reversibility of the sorption reaction. The fraction desorbed (D) is found by subtracting from unity the ratio of Cs concentration on the mica at the sampling time (t) to the Cs concentration on the mica at the start of the desorption process. Then, multiply by 100 for a percentage desorbed value.

$$D = 1 - \frac{[Cs]_{(t),mica}}{[Cs]_{(i),mica}} \times 100\% \quad (16)$$

Where *D* represents the fraction desorbed as a percentage value, $[Cs]_{(t),\ mica}$ represents the concentration of cesium on the mica at the sampling time *t* in dpm/g, and $[Cs]_{(i),\ mica}$ represents the concentration of cesium on the mica at the beginning of the desorption period in dpm/g.

2.10 Scanning Electron Microscopy and Energy-Dispersive X-Ray Spectroscopy

A sample of the muscovite was visualized using a Hitachi Field Emission SU-6600 scanning electron microscope (SEM) at Clemson University. The gun voltage of the SEM was 20

keV, and the sample was imaged as uncoated, directly placed on carbon tape. Semi-quantitative analyses using energy-dispersive X-ray spectroscopy were conducted for a selection of the SEM images obtained.

3 RESULTS

3.1 Sample Sieving

The particle size distribution for the bulk sample is reported below in Table 2 (below):

Table 2: Particle Size Distribution Results from Sample Sieving			
Sieve Size (U.S. Standard)	Sieve Size (mm)	Bulk Sample Mass (g)	Percent Distribution (wt. %)
No. 10	2.00	0	0
No. 20	0.841	0	0
No. 60	0.250	0.04	8
No. 325	0.044	0.38	76
Pan	< 0.044	0.06	12

Percent distribution values were determined according to Equation 1 (Section 2.3). From the data presented in Table 2, 8% of bulk sample particles have a diameter ranging from 0.250 mm to 0.841 mm. The majority (76%) of bulk sample particles are between 0.044 mm and 0.250 mm in diameter, and 12% of bulk sample particles are smaller than 0.044 mm in diameter.

3.2 X-Ray Diffractometry

The diffraction scan for the powdered sample is shown in Figure 5 (below). This test material is composed of muscovite, kaolin group minerals, and quartz. The semi-quantitative abundances of these minerals were determined as: 76% muscovite, 21% kaolin group, and 3% quartz per phase determination using PANalytical's HighScore Semi-Quantitative Analyses.

Each d-spacing value in Figure 5 (below) is paired with the single letter abbreviation for the mineral identity with which it corresponds, as determined via comparison against reference d-spacing values published by M.L. Jackson of the University of Wisconsin (Jackson, 1985) and by Moore and Reynolds (1997). A complete table of d-spacing values for the powdered sample with corresponding mineral identities per d-spacing value is included in the Appendix A.

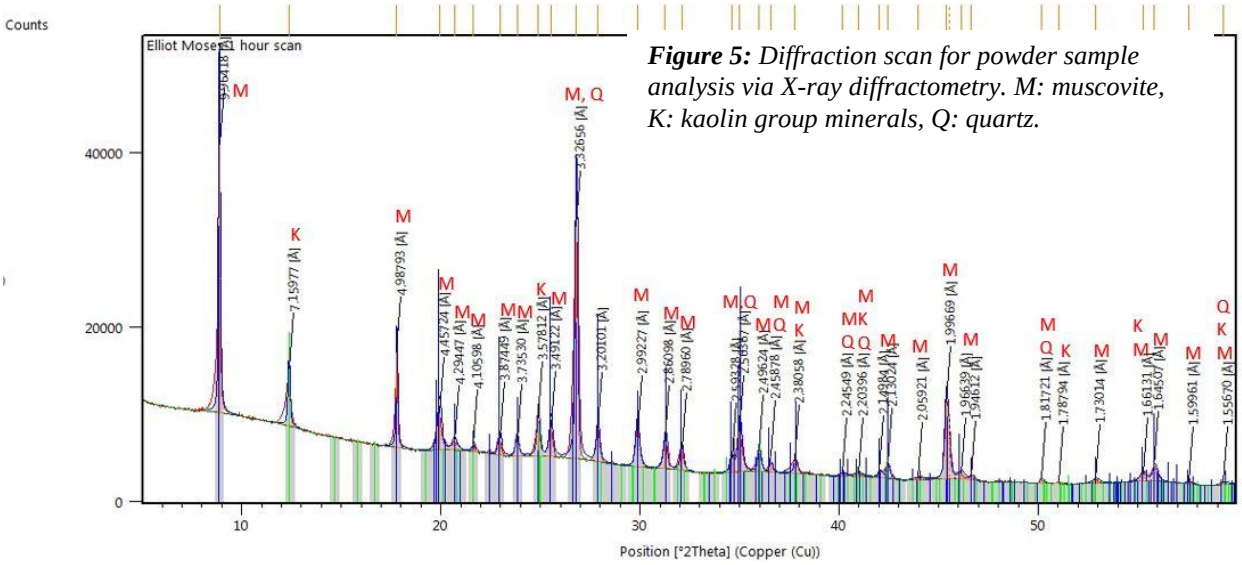

Figure 5: *Diffraction scan for powder sample analysis via X-ray diffractometry. M: muscovite, K: kaolin group minerals, Q: quartz.*

The diffraction scans of the < 2 μm particle diameter materials prepared as an oriented mount on a glass petrographic slide are shown in Figures 6 and 7 (below). Muscovite and kaolin group minerals are the predominant minerals seen in the < 2 μm particle diameter materials.

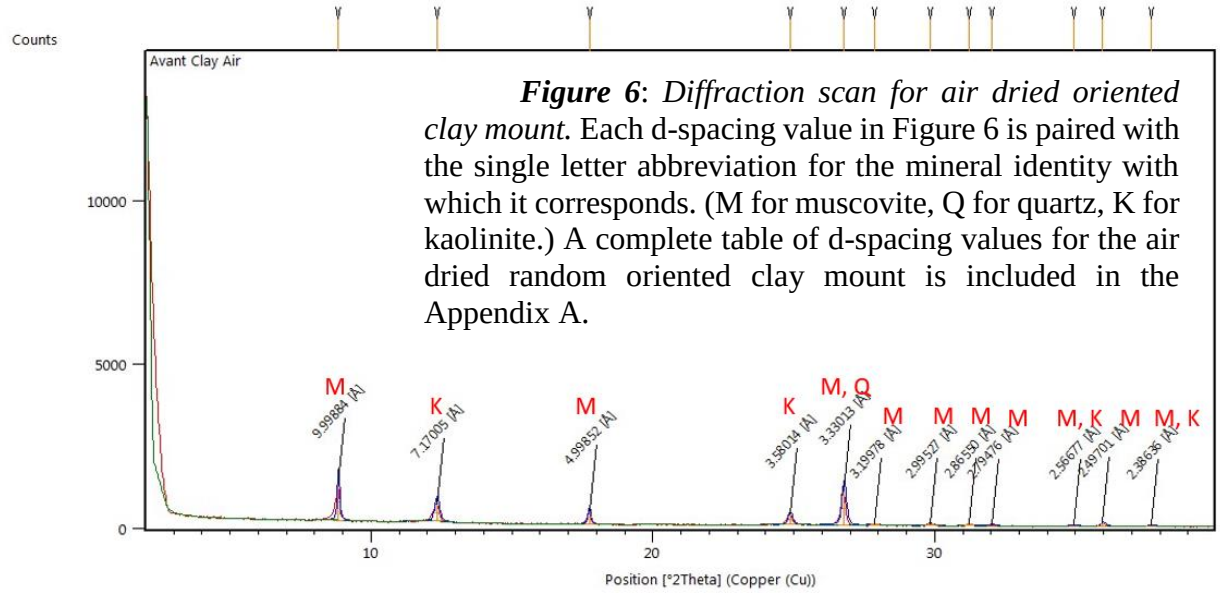

Figure 6: *Diffraction scan for air dried oriented clay mount.* Each d-spacing value in Figure 6 is paired with the single letter abbreviation for the mineral identity with which it corresponds. (M for muscovite, Q for quartz, K for kaolinite.) A complete table of d-spacing values for the air dried random oriented clay mount is included in the Appendix A.

This air-dried clay mount was created to test for the presence of smectite via comparison against an ethylene glycol random oriented mount, multi-layer clays and vermiculite. There was

no change observed for the < 2 μm particle diameter test materials after being solvated in ethylene glycol vapor (Figure 7, below).

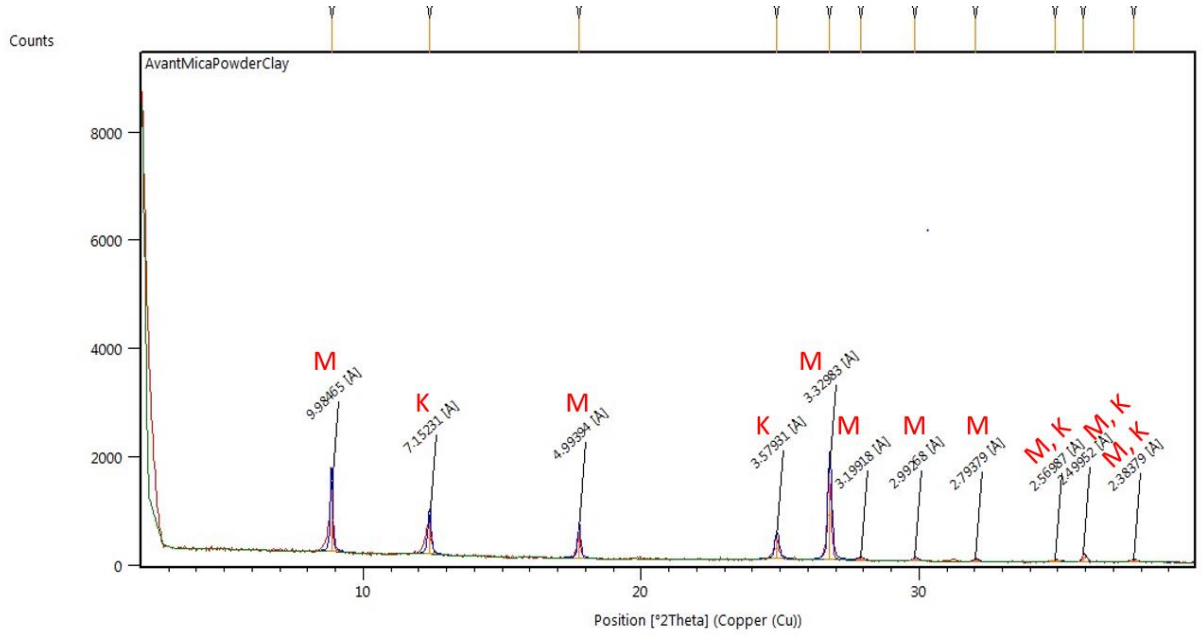

Figure 7: *Diffraction scan for ethylene glycol solvated random oriented clay mount. Symbols used as described in Figure 6.*

3.3 Strong Acid Extraction with HNO_3

Tables 3a and *3b (below)* showed the concentrations of Cs, Rb and K in the muscovite sample materials (crushed and as-is, respectively). Concentrations of Cs, Rb and K are reported in units of ng/g. These samples were treated with 70% nitric acid for 4 hours at 70º C. K was the most abundant element measured in these leachates from the crushed muscovite (156,000 - 177,100 ng/g). Cs was the least abundant element measured (18.9-21.6 ng/g). Rb concentrations varied from 586-664 ng/g. Table 3b showed the concentrations of Cs, Rb, K in the as-is (not crushed) mica sample, as measured per ICP-MS at Clemson University. K was the most abundant,

with concentrations varying from 5,690-7,197 ng/g. Cs was the least abundant, with concentrations varying from 9.8-13.1 ng/g. The concentration of Rb varied from 31.0-39.3 ng/g.

Table 3a: Concentrations of Cs, Rb, and K in Crushed Muscovite Sample of Leachates from Acid Leaching

Aliquot ID	Measured Cs (ng/g)	RSD of Measured Cs (%)	Measured Rb (ng/g)	RSD of Measured Rb (%)	Measured K (ng/g)	RSD of Measured K (%)
1	19.7	2.4	631	2.1	168900	2.3
2	20.9	0.7	658	0.7	174800	0.1
3	21.6	2.0	664	2.3	177100	1.8
4	18.9	0.4	586	0.3	156100	0.4
Average	20.275	1.375	634.75	1.35	169225	1.15
Blank M	1.0	0.5	0.1	2.0	22.0	8.3
Blank N	1.0	1.9	0.1	2.8	18.8	12.0

Table 3b: Concentrations of Cs, Rb, and K in As-Is Muscovite Sample of Leachates from Acid Leaching

Aliquot ID	Measured Cs (ng/g)	RSD of Measured Cs (%)	Measured Rb (ng/g)	RSD of Measured Rb (%)	Measured K (ng/g)	RSD of Measured K (%)
5	10.9	0.5	32.8	0.2	5890	0.7
6	11.9	0.5	37.2	0.5	6799	0.6
7	13.1	0.5	39.3	0.6	7197	0.5
8	9.8	0.6	31.0	0.1	5690	0.7
Average	11.425	0.525	35.075	0.35	6394	0.625
Blank M	1.0	0.5	0.1	2.0	22.0	8.3
Blank N	1.0	1.9	0.1	2.8	18.8	12.0

3.4 Major and Trace Element Analyses by Activation Laboratories, Ltd.

The concentrations of major elements of the muscovite (as received and split) are shown in Table 4 (below) as weight percent oxides. The sum of the major elements including LOI is 99.24 wt. %. The wt. % K_2O for the test muscovite appears to be low relative to wt. % K_2O known for a known muscovite (11.81 wt. %). The results for the concentrations of Cs, Rb, and K for are given in Table 5 in units of µg/g. The complete report of analysis is given in the Appendix B of this report.

Table 4: Major Element Analyses	
Oxide	Muscovite test material (wt. % oxide)
Na_2O	0.52
K_2O	7.51
SiO_2	46.78
Al_2O_3	34.24
Fe_2O_3	1.57
MgO	0.55
TiO_2	0.883
CaO	0.02
MnO	0.014
P_2O_5	0.03
LOI	7.11
Total + LOI	99.117

Table 5: Concentrations of Cs, Rb and K for Muscovite	
Analyte	Muscovite test material (µg/g)
Cs	245
Rb	3.0
K	62344

3.5 Fractions Extractable

The acid extractable fractions (F_{M+}) of Cs, Rb and K from the muscovite have been calculated according to the procedure in Section 2.7 and are reported in Table 6 (below):

Table 6: Fractions Cs, Rb, K Acid Extractable from Muscovite	
Analyte	Fraction Extractable (%)
Cs	0.04
Rb	1.03
K	0.09

3.6 Batch Sorption Experiments

The sorption of radioactive cesium (^{137}Cs) onto the muscovite was observed from LSC after 18 hours, 60 days, and 130 days of tumbling. The liquid phase ^{137}Cs concentration is obtained directly from LSC measurement. Solid phase ^{137}Cs is calculated from the difference between the quantity of added ^{137}Cs and measured ^{137}Cs in the aqueous phase, according to the equations in Section 2.8 that use ^{137}Cs concentrations instead of Cs concentrations.

While the results of batch sorption experimentation describe the partitioning of total cesium into the aqueous and solid phases, the results of ICP-MS measurements are not reported. Instead, the distribution of total Cs in the aqueous and solid phases is assumed to be equivalent to the distribution of ^{137}Cs between the two phases.

Tables 7a, 7b and 7c (below) present the aqueous and solid phase concentrations of Cs as calculated from the LSC data for the three sampling events (18 hours, 60 days and 130 days, respectively). Tables 7a, 7b and 7c also include the K_d values for each batch sorption test portion at 18 hours, 60 days and 130 days and the concentration of total Cs in each batch sorption test portion. Note that samples 11a and 11b are blanks, containing no ^{137}Cs and no ^{133}Cs.

Table 7a: Results for batch sorption experimentation as calculated from LSC data after 18 hours of tumbling

Sample ID	$[Cs]_{aq}$ (mol/L)	$[Cs]_{solid}$ (mol/kg)	Total [Cs] (mol/L)	K_d (mL/g)
1a	1.06×10^{-8}	1.57×10^{-5}	2.20×10^{-7}	1.49×10^{3}
2a	2.39×10^{-8}	4.66×10^{-5}	5.00×10^{-7}	1.95×10^{3}
3a	4.36×10^{-8}	9.72×10^{-5}	1.00×10^{-6}	2.23×10^{3}
4a	2.43×10^{-7}	4.52×10^{-4}	5.00×10^{-6}	1.86×10^{3}
5a	4.59×10^{-7}	9.32×10^{-4}	1.00×10^{-5}	2.03×10^{3}
6a	2.15×10^{-6}	4.55×10^{3}	5.00×10^{-5}	2.11×10^{3}
7a	4.92×10^{-6}	9.36×10^{3}	1.00×10^{-4}	1.90×10^{3}
8a	1.91×10^{-7}	3.14×10^{-4}	5.00×10^{-6}	1.64×10^{3}
9a	4.60×10^{-7}	9.65×10^{-4}	1.00×10^{-5}	2.10×10^{3}
10a	2.38×10^{-6}	4.81×10^{3}	5.00×10^{-5}	2.02×10^{3}

1b	7.90×10^{-9}	1.96×10^{-5}	2.20×10^{-7}	2.48×10^{3}
2b	2.08×10^{-8}	4.56×10^{-5}	5.00×10^{-7}	2.20×10^{3}
3b	3.57×10^{-8}	8.30×10^{-5}	1.00×10^{-6}	2.33×10^{3}
4b	2.10×10^{-7}	3.72×10^{-4}	5.00×10^{-6}	1.77×10^{3}
5b	4.46×10^{-7}	7.97×10^{-4}	1.00×10^{-5}	1.79×10^{3}
6b	2.46×10^{-6}	4.91×10^{3}	5.00×10^{-5}	1.99×10^{3}
7b	4.76×10^{-6}	9.90×10^{3}	1.00×10^{-4}	2.08×10^{3}
8b	2.46×10^{-7}	4.82×10^{-4}	5.00×10^{-6}	1.96×10^{3}
9b	4.29×10^{-7}	7.76×10^{-4}	1.00×10^{-5}	1.81×10^{3}
10b	2.38×10^{-6}	4.50×10^{3}	5.00×10^{-5}	1.89×10^{3}

Table 7b: Results for batch sorption experimentation as calculated from LSC data after 60 days of tumbling

Sample ID	$[^{137}Cs]_{aq}$ (mol/L)	$[^{137}Cs]_{solid}$ (mol/kg)	Total [Cs] (mol/L)	K_d (mL/g)
1a	1.93×10^{-9}	1.30×10^{-5}	2.20×10^{-7}	6.74×10^{3}
2a	1.70×10^{-8}	3.77×10^{-5}	5.00×10^{-7}	2.22×10^{3}
3a	1.78×10^{-8}	7.99×10^{-5}	1.00×10^{-6}	4.48×10^{3}
4a	1.66×10^{-7}	3.71×10^{-4}	5.00×10^{-6}	2.23×10^{3}
5a	4.69×10^{-7}	7.44×10^{-4}	1.00×10^{-5}	1.59×10^{3}
6a	2.79×10^{-6}	3.62×10^{3}	5.00×10^{-5}	1.30×10^{3}
7a	6.50×10^{-6}	7.51×10^{3}	1.00×10^{-4}	1.16×10^{3}
8a	1.11×10^{-7}	2.58×10^{-4}	5.00×10^{-6}	2.32×10^{3}
9a	4.55×10^{-7}	7.72×10^{-4}	1.00×10^{-5}	1.69×10^{3}
10a	3.05×10^{-6}	3.83×10^{3}	5.00×10^{-5}	1.25×10^{3}
1b	3.24×10^{-9}	1.60×10^{-5}	2.20×10^{-7}	4.93×10^{3}
2b	6.65×10^{-9}	3.75×10^{-5}	5.00×10^{-7}	5.63×10^{3}
3b	9.64×10^{-9}	6.81×10^{-5}	1.00×10^{-6}	7.06×10^{3}
4b	1.54×10^{-7}	3.05×10^{-4}	5.00×10^{-6}	1.97×10^{3}
5b	4.33×10^{-7}	6.39×10^{-4}	1.00×10^{-5}	1.48×10^{3}
6b	3.04×10^{-6}	3.92×10^{3}	5.00×10^{-5}	1.29×10^{3}
7b	6.32×10^{-6}	7.95×10^{3}	1.00×10^{-4}	1.26×10^{3}
8b	2.62×10^{-7}	3.88×10^{-4}	5.00×10^{-6}	1.48×10^{3}
9b	3.79×10^{-7}	6.23×10^{-4}	1.00×10^{-5}	1.64×10^{3}
10b	3.02×10^{-6}	3.58×10^{3}	5.00×10^{-5}	1.19×10^{3}

Table 7c: Results for batch sorption experimentation as calculated from LSC data after 130 days of tumbling

Sample ID	$[^{137}Cs]_{aq}$ (mol/L)	$[^{137}Cs]_{solid}$ (mol/kg)	Total [Cs] (mol/L)	K_d (mL/g)
1a	9.63E-10	1.14×10^{-5}	2.20×10^{-7}	1.18×10^{4}
2a	1.10×10^{-8}	3.34×10^{-5}	5.00×10^{-7}	3.03×10^{3}
3a	7.34×10^{-9}	7.06×10^{-5}	1.00×10^{-6}	9.61×10^{3}

4a	1.04×10^{-7}	3.31×10^{-4}	5.00×10^{-6}	3.18×10^{3}
5a	3.15×10^{-7}	3.31×10^{-4}	1.00×10^{-5}	2.10×10^{3}
6a	2.61×10^{-6}	3.20×10^{3}	5.00×10^{-5}	1.23×10^{3}
7a	6.21×10^{-6}	6.68×10^{3}	1.00×10^{4}	1.07×10^{3}
8a	6.13×10^{-8}	3.31×10^{-4}	5.00×10^{-6}	3.74×10^{3}
9a	4.01×10^{-7}	6.78×10^{-4}	1.00×10^{-5}	1.69×10^{3}
10a	2.89×10^{-6}	3.38×10^{3}	5.00×10^{-5}	1.17×10^{3}
1b	2.42×10^{-9}	1.40×10^{-5}	2.20×10^{-7}	5.79×10^{3}
2b	2.08×10^{-9}	3.31×10^{-5}	5.00×10^{-7}	1.59×10^{4}
3b	5.06×10^{-9}	5.98×10^{-5}	1.00×10^{-6}	1.18×10^{4}
4b	6.40×10^{-8}	2.74×10^{-4}	5.00×10^{-6}	4.28×10^{3}
5b	2.25×10^{-7}	5.71×10^{-4}	1.00×10^{-5}	2.53×10^{3}
6b	2.96×10^{-6}	3.46×10^{3}	5.00×10^{-5}	1.17×10^{3}
7b	5.89×10^{-6}	7.08×10^{3}	1.00×10^{4}	1.20×10^{3}
8b	1.73×10^{-7}	3.47×10^{-4}	5.00×10^{-6}	2.01×10^{3}
9b	2.32×10^{-7}	5.53×10^{-4}	1.00×10^{-5}	2.38×10^{3}
10b	2.78×10^{-6}	3.17×10^{3}	5.00×10^{-5}	1.14×10^{3}

Figure 8 (below) plots the concentration of solid phase Cs in units of mol/kg against the concentration of aqueous phase Cs in units of mol/L for the three sampling events (18 hours, 60 days and 130 days). The ratio of solid phase Cs to aqueous phase Cs appears to be increasing with time. In Figure 9 (below), the K_d value (calculated from Equation 5) for each batch sample test portion is plotted against the concentration of total Cs in the corresponding test portion. The K_d values increased with time. Additionally, an inverse relation was noted between the K_d values and the concentrations of total Cs in the test portion.

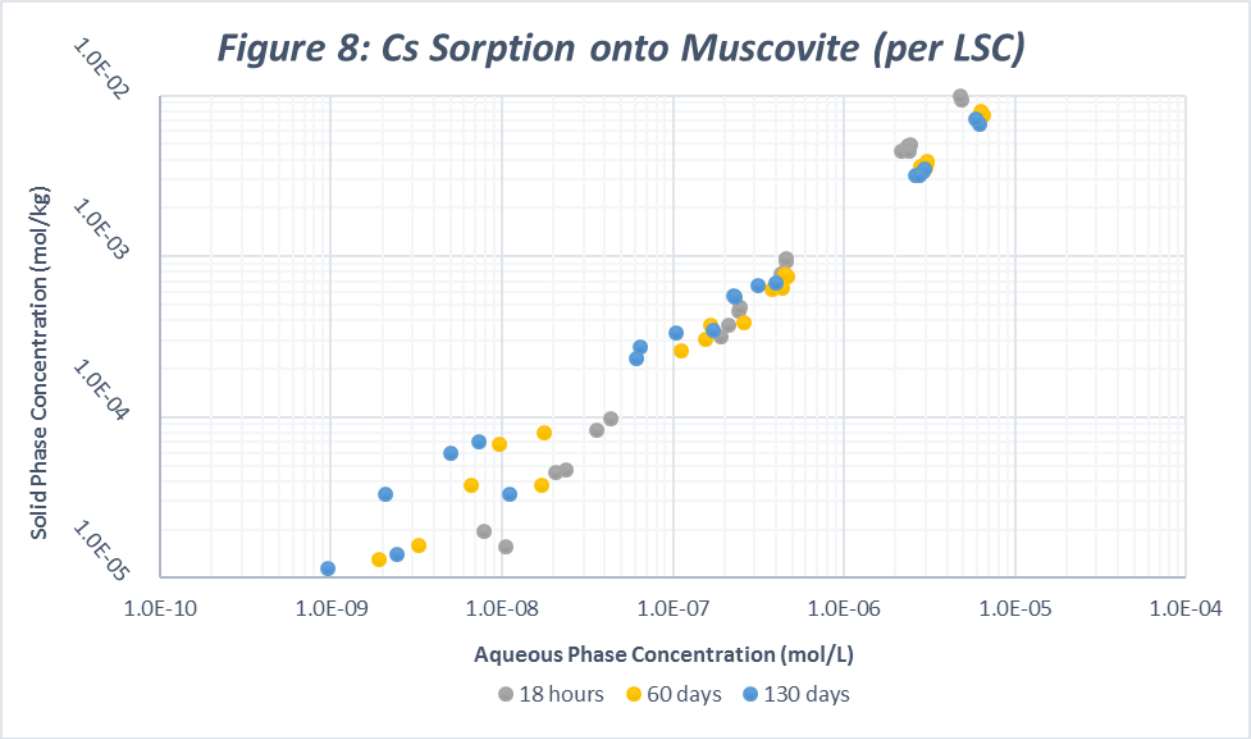
Figure 8: Cs Sorption onto Muscovite (per LSC)
Solid Phase Concentration (mol/kg)
1.0E-02
1.0E-03
1.0E-04
1.0E-05
1.0E-10
1.0E-09
1.0E-08
1.0E-07
1.0E-06
1.0E-05
1.0E-04
Aqueous Phase Concentration (mol/L)
18 hours
60 days
130 days

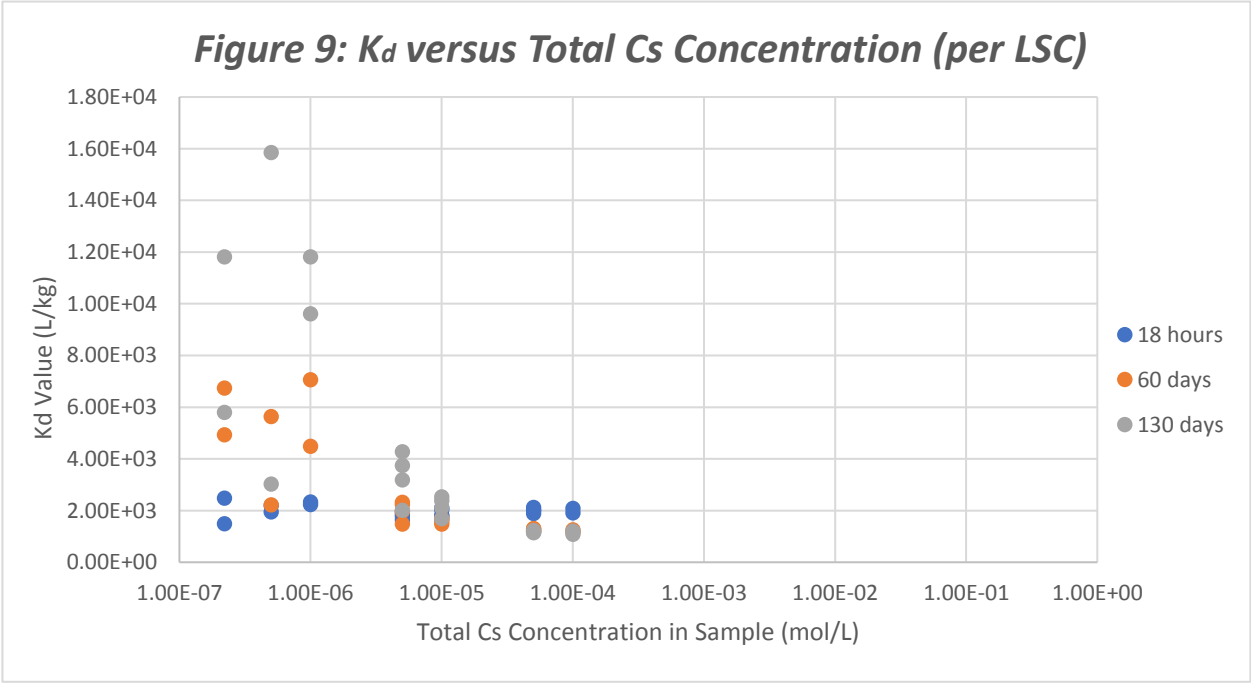
Figure 9: Kd versus Total Cs Concentration (per LSC)
Kd Value (L/kg)
1.80E+04
1.60E+04
1.40E+04
1.20E+04
1.00E+04
8.00E+03
6.00E+03
4.00E+03
2.00E+03
0.00E+00
1.00E-07
1.00E-06
1.00E-05
1.00E-04
1.00E-03
1.00E-02
1.00E-01
1.00E+00
Total Cs Concentration in Sample (mol/L)
18 hours
60 days
130 days

3.7 Batch Desorption Experiments

Following 130 days of batch sorption experimentation, desorption test portions were created from sorption test portions by centrifugation and decanting of the supernatant liquid. The supernatant liquid was replaced with a solution of NaCl (10 mM NaCl in portions 1a-10a; 1mM NaCl in portions 1b-10b) to introduce Na^+ as a counterion. These desorption test portions were tumbled for 60 days, then centrifuged, sampled, and yielded the following data.

Table 8a: Desorption using 10 mM NaCl after 60 days

Sample ID	$[Cs^{137}]_{mica}$ (dpm/g)	$[Cs^{137}]_{aq}$ (dpm/mL)	Initial $[Cs^{137}]_{mica}$ (dpm/mL)	Fraction Desorbed (%)	Measured Desorption Kd (mL/g)
1a	1134264	-1.997203915	21923.5507	-0.023	-5.68×10^5
2a	1448065	7.055029228	21721.8291	0.079	2.05×10^5
3a	1526636	42.21954162	21719.69803	0.464	3.62×10^4
4a	1375457	21.97363164	20807.44759	0.241	6.26×10^4
5a	1438303	36.96303696	21837.47091	0.417	3.89×10^4
6a	1328507	78.87380192	20940.89259	0.891	1.68×10^4
7a	1315134	122.0722509	19972.22575	1.378	1.08×10^4
8a	942148	135.9184489	20830.32595	1.476	6.93×10^3
9a	1462142	34.8987935	21635.71873	0.389	4.19×10^4
10a	1403346	72.5440806	20923.30064	0.826	1.93×10^4

Table 8b: Desorption using 1 mM NaCl after 60 days					
Sample ID	**$[Cs^{137}]_{mica}$ (dpm/g)**	**$[Cs^{137}]_{aq}$ (dpm/mL)**	**Initial $[Cs^{137}]_{mica}$ (dpm/mL)**	**Fraction Desorbed (%)**	**Measured Desorption K_d (mL/g)**
1b	1402067	0.998601957	22021.07636	0.011	1.40×10^6
2b	1437985	12.01682355	21780.69876	0.132	1.20×10^5
3b	1306046	10.04520342	21867.47289	0.109	1.30×10^5
4b	1146762	11.0486139	20987.09009	0.118	1.04×10^5
5b	1241631	24.97752023	21800.52838	0.276	4.97×10^4
6b	1430943	25.06014435	20756.13034	0.284	5.71×10^4
7b	1412043	70.92907093	20093.639	0.784	1.99×10^4
8b	1441718	90.22556391	20959.43585	1.000	1.60×10^4
9b	1184690	42	21508.9732	0.472	2.82×10^4
10b	1325813	31.05268606	21010.93898	0.351	4.27×10^4

Tables 8a and 8b (above) present data collected from 60 days of desorption for test portions containing 10 mM NaCl and 1 mM NaCl, respectively. Tables 8a and 8b present the concentrations of ^{137}Cs in the aqueous phase, as measured by LSC and normalized to the volume of NaCl in each test portion. The concentration of ^{137}Cs in the solid phase is calculated as the difference between the measured aqueous ^{137}Cs and the original concentration of ^{137}Cs on the mica at the start of the desorption period. The quantities for fraction desorbed, as presented in Tables 8a and 8b, are calculated according to Equation 16 in Section 2.9. The K_d values presented in Tables 8a and 8b are calculated according to Equation 15 in Section 2.9.

Note that no data is reported for batch desorption test portions 11a and 11b, because batch desorption test portions 11a and 11b were blanks containing mica, but no stable cesium or radiocesium.

Figure 10 (below) plots the K_d in units of (L/kg) against the initial concentration of total Cs in mol/L. The data is presented in a logarithmic scale, allowing for differentiation of the two

groups of batch desorption test portions—one group of test portions containing 10 mM NaCl; the other containing 1 mM NaCl. The K_d value for the lowest stable Cs test portion with 10 mM NaCl (Sample 1a) could not be calculated. The measured LSC for this sample was < 0 (Table 8a).

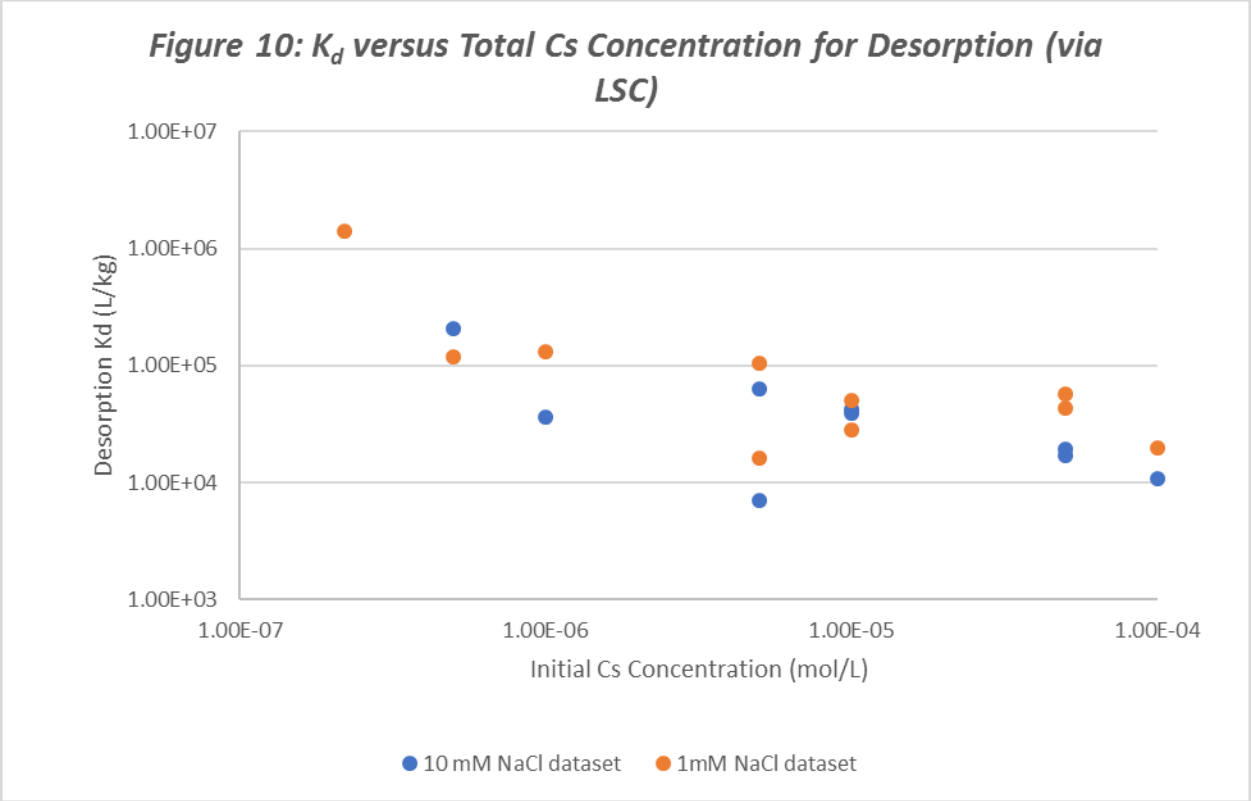

3.8 Scanning Electron Microscopy and Energy-Dispersive X-Ray Spectroscopy

The following images (Figures 11-15) were obtained from imaging the uncoated muscovite using a Hitachi Field Emission SEM SU-6600 with 20 keV gun voltage. Semi-quantitative analyses using energy-dispersive X-ray spectroscopy (EDS) are included for Figures 11-13.

Figure 11 (below) showed a view down the c-axis of one muscovite flake. Evidence of extensive weathering visible, manifesting as stair-step patterns of the image. These stair step patterns may be the result of a partial removal of either tetrahedral or octahedral sheet.

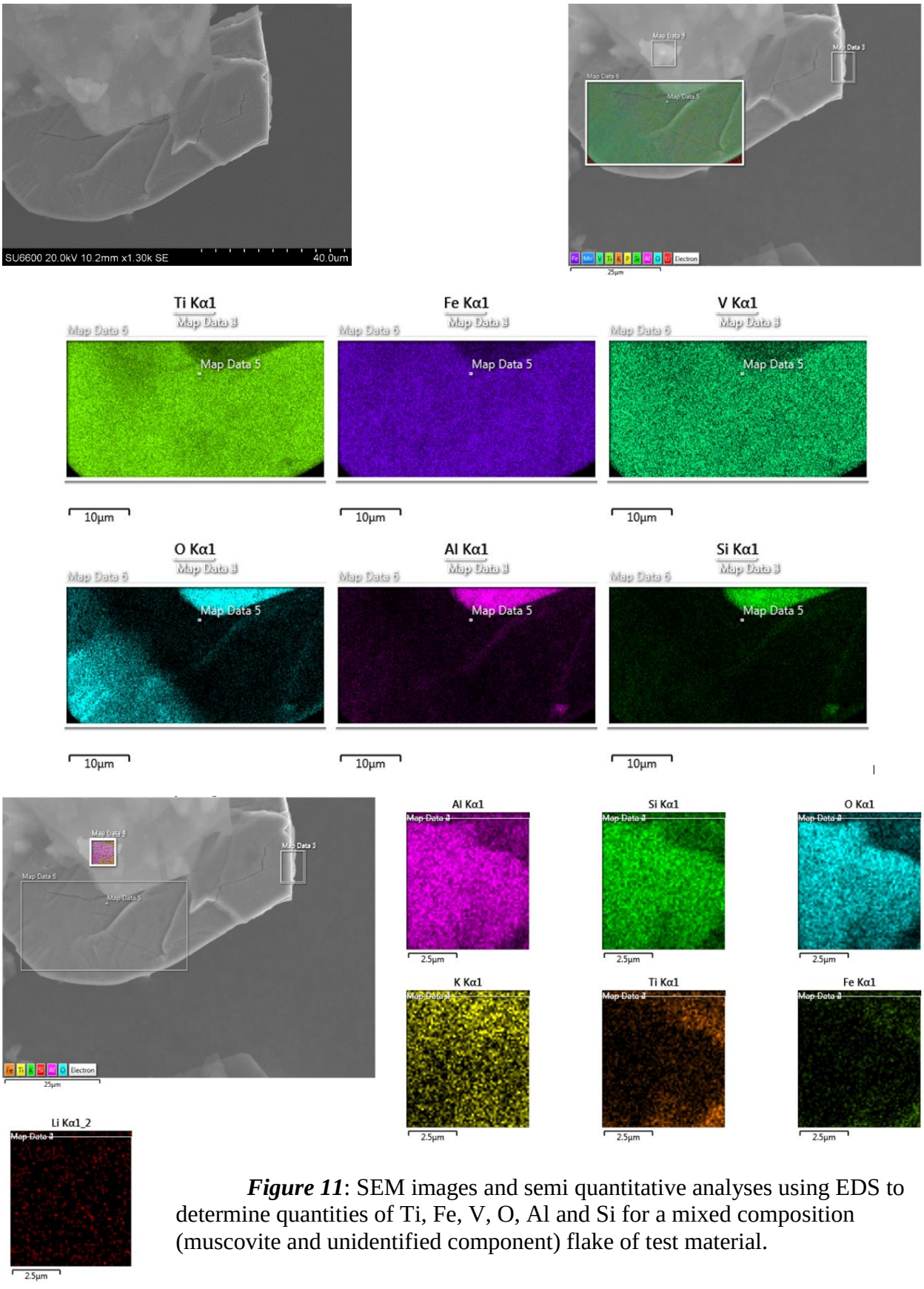

Figure 11: SEM images and semi quantitative analyses using EDS to determine quantities of Ti, Fe, V, O, Al and Si for a mixed composition (muscovite and unidentified component) flake of test material.

Weathering, as such, may have created additional binding sites for ^{137}Cs—perhaps directly on the edges of each stair-step shown in Figure 11. Such binding sites would undoubtedly contribute to the Freundlich-nature of the sorption isotherms described in Sections 2.8 and 3.6.

Figure 11 (above) showed SEM images and semi quantitative analyses for a mixed composition flake of test material. Two regions of interest were examined. The first region of interest is located on the bottom "shelf" of the stair-step configuration. From semi-quantitative analysis, potassium was not a significant element found in this region of the flake. Therefore, assuming that potassium is primarily held in the interlayer of muscovite, the lack of potassium indicates that this region is not muscovite.

The second region of the muscovite is located on the "higher" portion of the flake's stair-step topography. Contrary to the first region of interest, the significant concentration of potassium present indicates that this portion of the flake may be muscovite.

Figure 12 (below) shows a near-oblique view of a muscovite flake, wherein various aberrations are visible on the surface of the flake. Again, this may be attributed to processes through which this muscovite was slaked. Again, there exists a possibility of specificity for radiocesium binding at any of these weathered sites. This view of the muscovite nearly shows the frayed edge sites at the extreme edges of the flake; however, no optimal view of an FES was obtained via SEM.

Figure 12 also includes semi-quantitative analyses generated via EDS to quantify O, Al, Si, K, Na, Ti, Fe and Li present within this flake of test material. The presence of significant amounts of potassium lends to the interpretation of this particular flake as muscovite, assuming that K is held within the interlayer of the mineral.

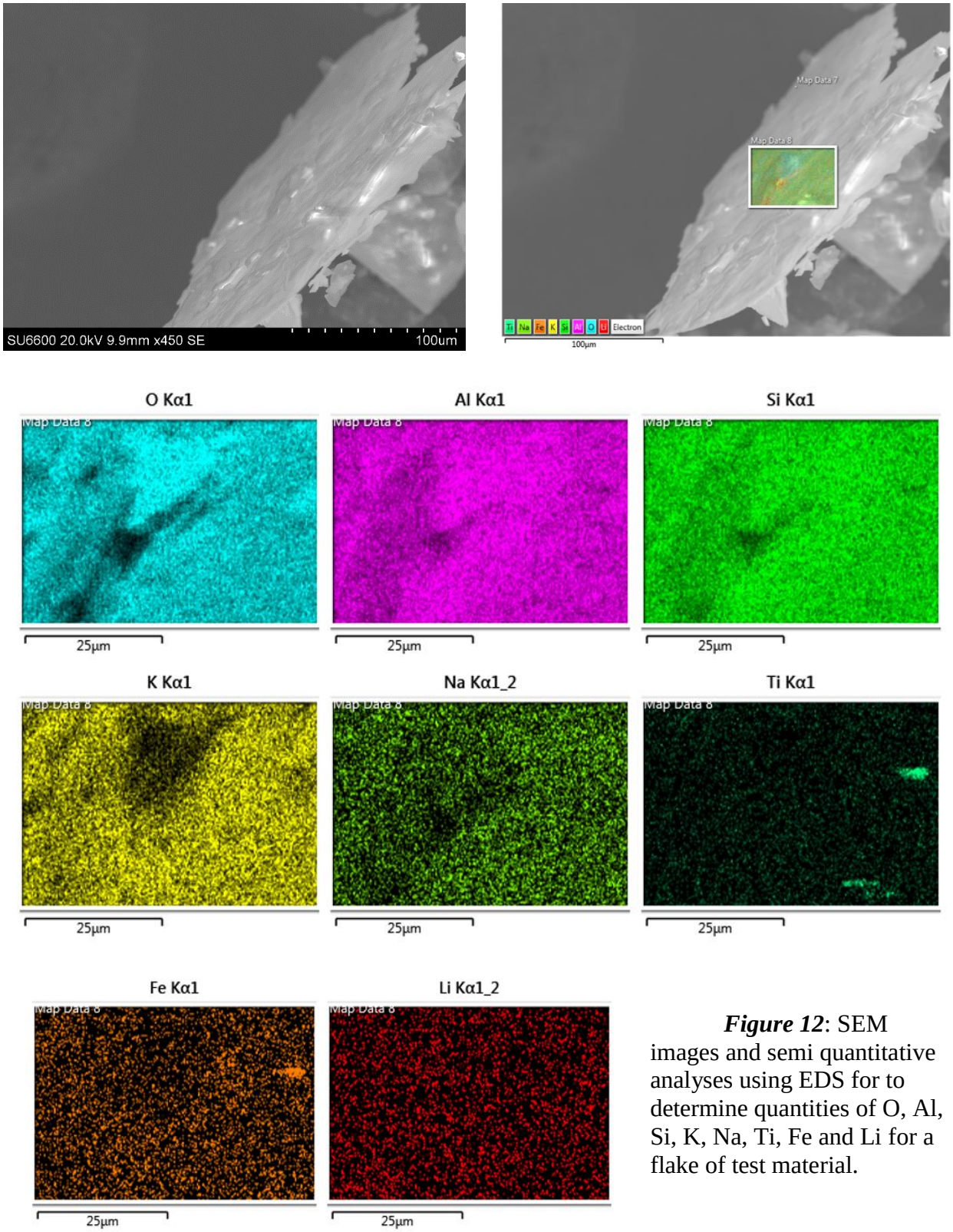

Figure 12: SEM images and semi quantitative analyses using EDS for to determine quantities of O, Al, Si, K, Na, Ti, Fe and Li for a flake of test material.

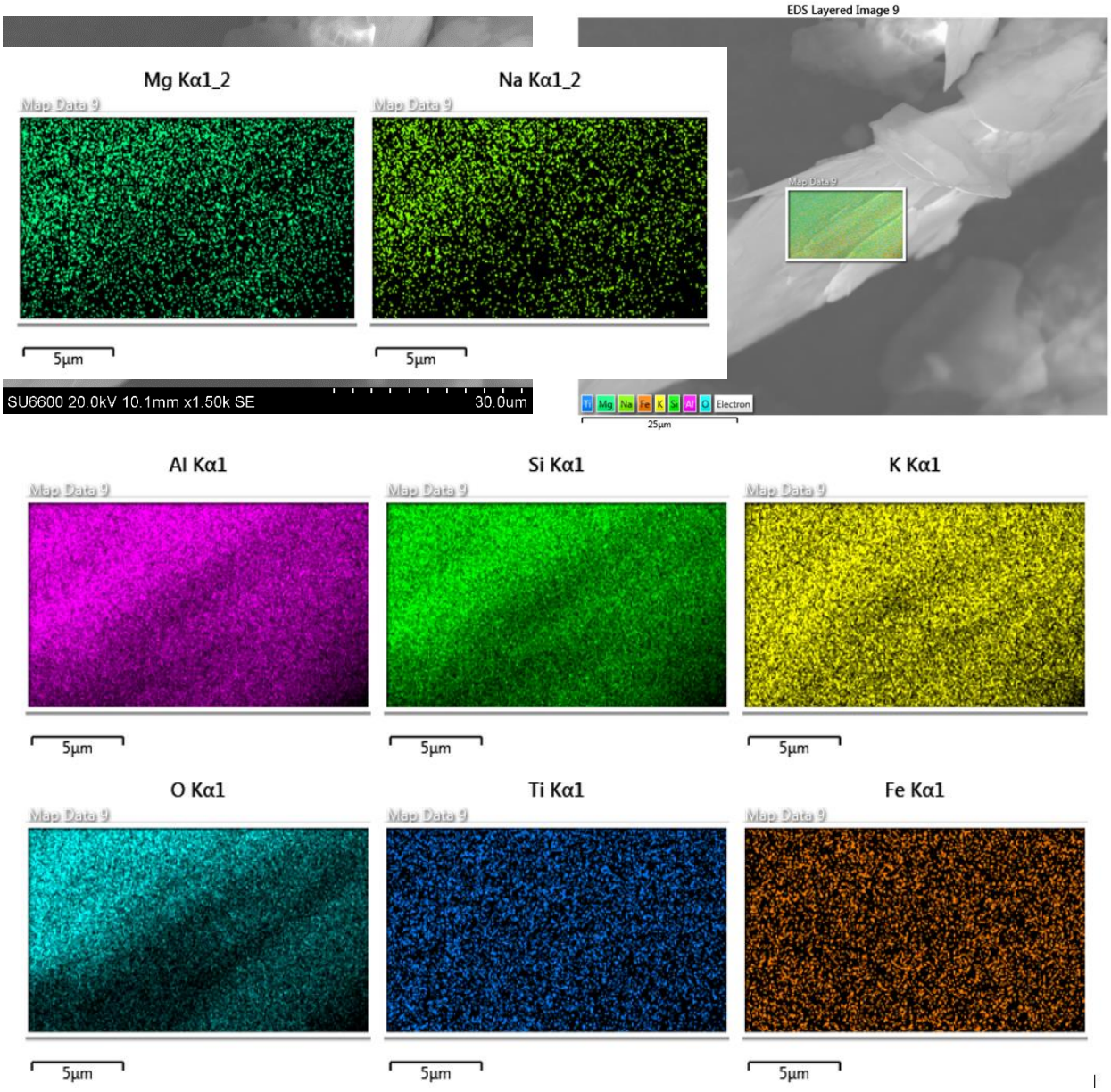

Figure 13: SEM images and semi quantitative analyses using EDS for to determine quantities of Al, Si, K, O, Ti, Fe, Mg, and Na for a flake of test material. The blue arrow in the top left image shows a frayed edge site (FES)

There may be several interpretations for the muscovite shown in Figure 13 (above). One such interpretation is that Figure 13 shows a muscovite flake that had been subjected to a bending moment. As a result, the flake has split incompletely and unevenly at the center of the image, revealing various smaller layers within the muscovite. In

the process, this weathering and bending moment may have created more sorption sites for radiocesium.

Again, the semi-quantitative yield of potassium in this particular flake shown in Figure 13 is indicative of a mica identity. Figures 14 and 15 (below) show SEM images of flakes without semi-quantitative analyses using EDS.

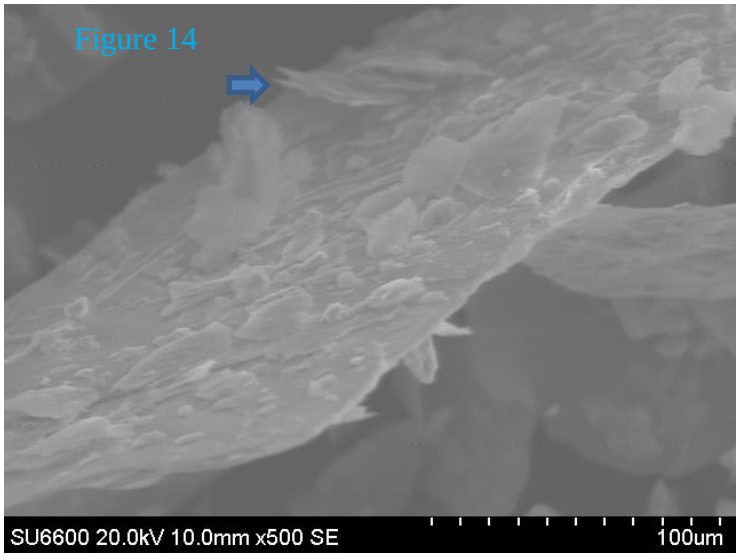

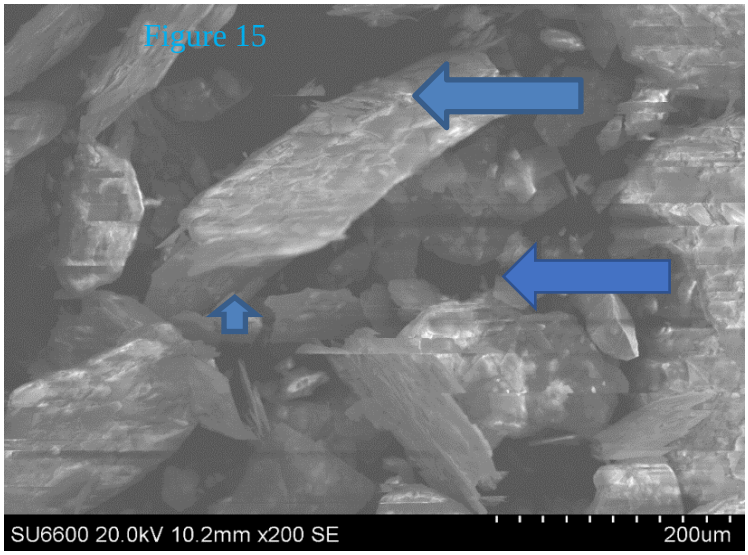

Figures 14 and 15 (left): *SEM images showing individual flakes of the bulk mica sample. No EDS semi-quantitative analyses are included for these SEM images. The blue arrows show frayed edges.*

4 DISCUSSION

4.1 Sample Sieving

Table 2 (Section 3.1) presents results from sieving a 0.5 g portion of the muscovite test portion. From Table 2, 8% of particles have a diameter greater than 0.250 mm and less than 0.841 mm. The majority (76%) of bulk sample particles are between 0.044 mm and 0.250 mm in diameter, and 12% of bulk sample particles are smaller than 0.044 mm in diameter. By convention, 84% of this material is comprised of sand-sized (0.050 mm) particles. This test material is of larger grain size than other illites or muscovites studied for ^{137}Cs sorption (e.g. Rajec et al., 1999) or powdered test materials (e.g. Clay Mineral Society Source Clay Materials).

4.2 X-Ray Diffractometery

Figure 5 (see section 3.2) showed the 1 hour diffraction scan from powder sample (15-minute crush) analysis. Phase determination via PANalytical's High Score Semi-Quantitative analyses yielded that the mica sample was composed of 76% muscovite ($2M_1$), 21% kaolinite ($1M_D$) and 3% quartz (low). Kaolinite and quartz are expected phases to be found in this type of material. The quartz and kaolinite have low cation exchange capacities. These phases would not be expected to sorb radiocesium, Cs, or Rb.

With respect to experimentally determined d-spacing values, the HighScore software indicated that the mineral dickite is a better match than kaolinite; however, based on the sample's original locality, the sample deductively contained kaolinite. The most intense diffraction peaks corresponding exclusively to nacrite (2.41Å) and dickite (2.32Å) were not observed (Moore and Reynolds, 1997). Kaolinite is the prevalent kaolin group mineral in this test material.

There was no appreciable difference between the d-spacing values obtained from the air-dried mount (Figure 6) versus those obtained from ethylene glycol solvated mount (Figure 7). Ethylene glycol solvation served as a primary test for the identification of smectite via X-ray diffraction (Moore and Reynolds, 1997). Organic solvents, chiefly ethylene glycol and glycerol, expand the inter-atomic sheet spaces (d-spacing values) of smectite clays (e.g.; montmorillonite, nontronite, beidellite, etc), mixed-layer clays and vermiculite (Jackson, 1985; Moore and Reynolds, 1997). Therefore, since the d-spacing values remain unchanged in the ethylene glycol solvated mount, the sample is unlikely to contain significant fractions of smectite. This solvation demonstrated also that mixed layer interstratified kaolinite-smectite (if present) interstratified minerals were not present in this sample. An evident assymetric peak on the high d-spacing side of the 001 peak for kaolinite was not observed. Kaolinite was not interlayered with other phyllosilicate minerals (muscovite).

4.3 Strong Acid Extraction with HNO_3

Tables 3a and 3b (Section 3.3) detailed the results of a strong acid extraction treatment on the muscovite mica sample. Treatment with hot, strong HNO_3 was intended to liberate metal ions from the muscovite test material to determine the extractable fractions of Cs, Rb and K. Table 3a specifically showed results of a strong acid extraction treatment of a 15-minute crush sample of the muscovite mica. Because this aliquot set was crushed, it appeared that more metal ions were extractable than if the sample were not crushed, as in Table 3b. Aliquots “M” and “N” in both Tables 3a and 3b represent method blanks. Smaller muscovite grains were more susceptible to chemical attack due to higher surface area.

4.4 Major and Trace Element Analyses by Activation Laboratories, Ltd.

Table 4 (Section 3.4) showed selected results from the major and trace element analyses (Package 8-REE, conducted by Activation Laboratories, Ltd.) as weight percent oxides of major elements. Table 5 (Section 3.4) showed the concentrations of Cs, Rb and K found in the muscovite in units of µg/g, for later use to determine fractions of Cs, Rb and K acid extractable from the interlayer of the muscovite (Sections 2.7, 3.5 and 4.5). Cesium was the least abundant element found in the leachates. Potassium was the most abundant ion found in the leachate. The low K contents of this muscovite is consistent with the low K contents of muscovite from the Georgia Kaolin deposits (Elser, 2004). Chemical weathering likely removed a significant portion of K from this muscovite test material as opposed to mineral separation and processing to create this test material.

4.5 Fractions Extractable

Table 6 (Section 3.5) showed the calculated fractions of Cs, Rb and K extractable from the muscovite test material. Cs, Rb, and K are understood to be interlayer cations in muscovite. These extractable were expressed as percentages. These values are calculated according to Equation 4 (Section 2.7) from the ratio of analyte extracted using 70% HNO_3 to the amount of analyte measured by Activation Laboratories, Ltd. Relatively negligible quantities of Cs, Rb and K were acid extractable (0.004%, 1.03%, and 0.009%, respectively), indicating that a negligible quantity of these cations are naturally present in the mineral to impact the results of batch sorption experimentation.

4.6 Batch Sorption Experiments

Figure 8 (Section 3.6) shows isotherms of radiocesium sorption onto muscovite as calculated from radiocesium measurements using LSC. In Figure 8, the aqueous phase

concentration of Cs in mol/L is plotted against solid phase concentration of Cs. The isotherms shown in Figure 8 represent three different data sets derived from the three sampling events occurring after 18 hours (grey dots), 60 days (yellow dots) and 130 days (blue dots) of continuous mechanical tumbling. The slope of a line from the origin (on a linear-scale plot, not shown) through these data points will express the ratio of the solid phase concentration of Cs (in mol/kg) to the aqueous phase concentration of Cs (in mol/L). This slope represented the distribution of Cs into the solid and aqueous phases (distribution coefficient K_d) in each batch sorption test portion.

Figure 8 appeared to show a trend of decreasing K_d values over time, fitting a Freundlich isotherm. These decreased Kd values support the idea of multiple binding sites in and on the muscovite surface (e.g. Goto et al., 2014; Durrant et al., 2018). Some of these binding sites have a higher affinity for Cs than others. In a kinetic model of sorption of Cs onto the test muscovite, the specific sites with higher affinity for Cs would, in theory, be filled first, accounting for the high K_d values observed at the beginning of the sorption period. An example of these high affinity sites might include the theoretical frayed edge site (FES), or sites within the muscovite interlayer (Zaunbrecher et al., 2015a, b). After the high affinity sites are filled within the FES, other exchangeable interlayer sites were filled. A third possible site was the siloxane surface that are able to weakly interact/sorb Cs, but with significantly lower affinity. Finally, the decrease in K_d value could be attributed to the kinetic processes or mass action, wherein there are now a lower quantity of sites (low affinity, or high affinity) able to sorb Cs and the rate of reaction is slowed accordingly.

It is important to note that batch sorption experiments in this study were not observed to reach equilibrium. However, K_d values for each test portion are calculated according to Equation 5 (Section 2.8) assuming an equilibrium was reached.

Calculated K_d values for batch sorption test portions are plotted against the concentration of total Cs in Figure 9 (Section 4.5). Figure 9 also highlighted the effect of sorbate concentration on the mica's sorption behavior. Generally speaking, as the concentration of total Cs added to each test portion was increased, the test portions appeared to approach equilibrium much faster, as evaluated in the change in K_d value per aliquot over time. K_d values for high [Cs] test portions seemed to change minimally as compared to low [Cs] test portions. For example, the test portions with the highest concentrations of total Cs (1.00×10^{-4} M and 5.00×10^{-5} M) showed decreases in average K_d values of 9.20×10^2 L/kg and 8.01×10^2 L/kg, respectively from the 1st sampling event (18 hours) to the 3rd sampling event (130 days).

For the test portions with the lowest two concentrations of total Cs (2.20×10^{-7} M and 5.00×10^{-7} M), K_d values increased on average by 6.81×10^3 L/kg and 7.39×10^3 L/kg, respectively from the 1st to the 3rd sampling events.

Generally speaking, there were large increases in K_d at low [Cs], but not at high [Cs]. This trend suggests that high [Cs] test portions are closer than low [Cs] test portions to reaching an equilibrium.

For the measurement of ^{137}Cs by LSC, it is inferred that a decreased K_d value results from a "sorbate equilibrium" wherein ^{137}Cs is being "bounced out" of the mica by ^{133}Cs, thus changing the concentration of aqueous ^{137}Cs measured via LSC and the K_d values calculated from these measurements.

4.7 Batch Desorption Experiments

Results from batch sorption experimentation yield K_d values ranged from 1.0×10^3 to 1.0×10^6 mL/g. Excluding the negative K_d values (derived as a result of background activity measurements by LSC), the results showed a strong correlation of decreased K_d for ^{137}Cs with

increased concentrations of added stable cesium. This correlation is due to stronger Cs sorption to a limited number of high affinity sites, which causes increased K_d at lower total cesium concentrations. This correlation held true for both the 1 mM and 10 mM NaCl batch desorption test portions.

Two different concentrations (1 mM and 10 mM) of NaCl were used in batch desorption test portions to examine the effect of counterion concentration on desorption behavior. K_d values are consistently smaller for the 10 mM NaCl test portions than for the 1 mM NaCl test portions due to mass action. A larger concentration of competing sodium cations leads to more "bouncing out" of cesium cations from binding sites on the mica.

Overall, K_d values derived for desorption are all large, meaning that very little ^{137}Cs is being desorbed from the mica. Large K_d values support practical industrial application for the muscovite.

4.8 Scanning Electron Microscopy and Energy-Dispersive X-Ray Spectroscopy

In attempts to visualize the test muscovite, an uncoated sample portion was subject to scanning electron microscopy (SEM). Figures 11-15 (Section 3.8) constitutesd a sample of images obtained via SEM.

With respect to the three varieties of binding sites present in phyllosilicate minerals, as described by Evans et al., (1983), the muscovite flake in Figure 11 displays several examples of planar sites for electrostatic and exchangeable radiocesium bonding.

Figures 12 and 13 show a muscovite flakes with a particularly prominent frayed edge site (FES), which qualifies as a type of interlayer binding site. Such interlayer sites typically contributed to strong sorption and fixation of radiocesium into the muscovite interlayer, wherein K^+ was formerly lost due to weathering processes.

Figures 14 and 15 show muscovite flakes with several examples of planar sites and frayed edge sites, contributing to exchangeable sorption, as well as fixation of radiocesium onto the bulk muscovite sample.

5 CONCLUSIONS

The following conclusions are derived from this study:

The muscovite test material was obtained from Southeastern Performance Minerals as a waste product of kaolin processing. The muscovite test material fraction consisted of 8% of the larger than 250 microns, 76% larger than 44 microns, and 12% was smaller than 44 microns. This test material is composed of 76% muscovite, 21% kaolinite, 3% quartz and 1% unidentified phases per semi-quantitative X-ray diffraction analyses. Kaolinite and quartz were not considered important in the sorption and desorption of radiocesium.

The muscovite is K-poor, relative to the known major element analyses of muscovite. Muscovite, $KAl_2(AlSi_3O_{10})(OH_2)$, typically contains about 11.81 wt. % K_2O. The K-poor quality of the muscovite can be attributed to excessive weathering. Substantial concentrations of K were released from the interlayer during chemical weathering in nature.

Batch sorption experiments in dilute a NaCl solution with varied concentrations of stable Cs, ^{137}Cs and Rb yielded increasing K_d values of radiocesium sorption per mass test material over time. The K_d values increased from 1.49×10^3 mL/g at the first sampling, to 1.59×10^4 mL/g in the third sampling. The K_d values also increased with decreasing concentrations of stable Cs. This dependence of K_d on stable Cs concentration was consistent with a Freundlich model isotherm.

Batch desorption experiments (60 days) in dilute NaCl solutions (1 mM and 10 mM) yielded likewise high K_d values, ranging from 6.93×10^3 mL/g to 1.40×10^6 mL/g. These high K_d values indicated that only a small fraction (0.011% - 1.476%) of the ^{137}Cs was removed from the mica by desorption. This fraction is smaller compared to recent values obtained by Durrant et al (2018). High K_d values as such suggest a fixation of ^{137}Cs onto the limited number of high affinity sites at the apex of the frayed edge site within the muscovite interlayer.

Batch sorption and desorption experimentation results generally support the three site models for radiocesium sorption onto clay minerals (Evans et al, 1983). These models describe three kinds of binding sites for radiocesium: 1) surface and planar sites, 2) wedge sites, and 3) interlayer sites.

SEM imaging helped visualization of possible high affinity sites for ^{137}Cs fixation by stressing the excessively weathered nature of the test muscovite. Several kinds of weathered sites were found at the edges and on the surfaces of mica flakes. The ideal view of a frayed edge site was not obtained via SEM at this time.

Further evidence supporting the existence of the observed sorption and desorption behavior of this test material warrants further study to show the utility of this mica as industrial /radionuclide sorbent applications.

6 FUTURE WORK

Possible endeavors for future experimentation on this muscovite fraction could include:

- To complete the sorption and desorption isotherms and to quantify the sorbent capacity of the muscovite, batch sorption and desorption experiments may be continued with more test portions over a longer tumbling period.
- Batch sorption and desorption experiments may be repeated using varied kinetic configurations.
- Atomic models of the sorption/fixation mechanism may be developed.
- SEM imaging of the muscovite may continue, especially to visualize high-affinity sites and to obtain an optimal view of frayed edge sites.

- Ion-exchange constants for the sorption of radiocesium onto the test muscovite may be calculation using the Vanselow model (Sposito).

REFERENCES

Carlton, W. H., Bauer, L. R., Evans, A. G., Geary, L. A. , Murphy, Jr., C. E., Pinder, J. E., and Storm, R. N. (1996). Cesium in the Savannah River Site Environment, Westinghouse Savannah River Company, Savannah River Site, Aiken, S.C, 29808, 96.

Cornell, R. M. Adsorption of Cesium on Minerals: A Review. Journal of Radioanalytical and Nuclear Chemistry. 1993. 171 (2), 483-500.

Cummins, C.L., C.S. Hetrick, D. K. Martin, 1991, "Radioactive Releases at the Savannah River Site 1954-1989", WSRC-RP-91-684, Westinghouse Savannah River Company, Aiken, SC.

Durrant, C., Begg, J., Kersting, A., Zavarin, M. Cesium sorption reversibility and kinetics on illite, montmorillonite, and kaolinite. Science of the Total Environment. 2018. 511-520.

Elser, A. M., The Provenance and Weathering of Muscovite from the Georgia Kaolin Deposits [Ph.D. thesis]: Atlanta: Georgia State University.

Environmental Protection Agency. (1996) Method 3050B, Acid Digestion of sediments, sludges, and soils, US Environmental Protection Agency, http://www.epa.gov/wastes/hazard/testmethods/sw846/pdfs/3050b.pdf

Evans, D. W., Alberts, J. J., Clark, R. A. Reversible ion-exchange fixation of cesium-137 leading to mobilization from reservoir sediments. Geochimica et Cosmochimica Acta. 1983. 47, 1041-1049.

Fuller, A., Shaw, S., Ward, M., et al. Caesium incorporation and retention in illite interlayers. Applied Clay Science. 2015. 128-134.

Goto, M.; Rosson, R.; Elliott, W. C.; Wampler, J. M.; Serkiz, S.; Kahn, B. Freundlich and Dual Langmuir Isotherm Models for Predicting ^{137}Cs Binding on Savannah River Site Soils. Health Physics. 2008. 94, 18-32.

Goto, M.; Rosson, R.; Elliott, W. C.; Wampler, J. M.; Serkiz, S.; Kahn, B. Interactions of Radioactive and Stable Cesium with Hydroxy-Interlayered Vermiculite Grains in Soils of the Savannah River Site, South Carolina, USA. Clays and Clay Minerals. 2014, 62, 161-173.

Grim, R. E. 1968. *Clay Mineralogy*, 2nd Ed. New York, New York: McGraw-Hill.

Ishikawa N. K; Kuwata, M; Ito, A; Umita T. Effect of pH and Chemical Composition of Solution on Sorption and Retention of Cesium by Feldspar, Illite and Zeolite as Cesium Sorbent from Landfill Leachate. Soil Science. 2017. 182 (2), 63-68.

Jackson, M. L. Soil Chemical Analysis—Advanced Course. 2nd ed.; M. L. Jackson: Madison, 1985.

Kogel, J. E.; Pickering, S. M.; Shelobolina, E.; Yuan, J.; Chowns, T. M.; Avant, D. M. Geology of the Commercial Kaolin Mining District of Central and Eastern Georgia; Georgia Geological Society Guidebooks; Georgia Geological Society: Carrolton, GA, 2000; pp 57-59.

Lee, J., Park, S., Jeon, E., Baek, K. Selective and irreversible adsorption mechanism of cesium on illite. Applied Geochemistry. (2017), http://d.doi.org/10.1016/j.apgeochem.2017.05.019

Moore, D. M; Reynolds R. C., Jr. 1997. X-Ray Diffraction and the Identification and Analysis of Clay Minerals, 2nd Ed. Xviii pp 378. Oxford, New York: Oxford University Press. ISBN 0 19 508713 5. Geological Magazine 1998, 135 (6), 819–842.

Prasad, M. S., Reid, K. J., Murray, H. H. Kaolin: processing, properties and applications. Applied Clay Science. 1991. (6), 87-119.

Rajec, P., Sucha, V., Eberl, D., Srodon, J., Elsass, F. 1999. "Effect of Illite Particle Shape on Cesium Sorption." Clays and Clay Minerals 47: 755-760.

Wampler, J. M., Eirik J. Krogstad, W. Crawford Elliott, Bernd Kahn, and Daniel I. Kaplan. 2012. "Long-Term Selective Retention of Natural Cs and Rb by Highly Weathered Coastal Plain Soils." Environmental Science and Technology 46: 3837–43. doi:10.1021/es2035834.

Yoshida, N., and Takahashi, Y., 2012, Land-Surface Contamination by Radionuclides from the Fukushima Daiichi Nuclear Power Plant Accident: Elements, vol. 8, 201-206

Zaunbrecher, L. K.; Cygan, R. T.; Elliott, W. C.; Molecular Models of Cesium and Rubidium Adsorption on Weathered Micaceous Minerals. J. Phys. Chem A. 2015. 119, 5691-5700.

Zaunbrecher, L. K.; Elliott, W. C.; Wampler, J. M.; Perdrial, N.; Kaplan, D. I. Enrichment of Cesium and Rubidium in Weathered Micaceous Materials at the Savannah River Site, South Carolina. Environ. Sci. Technol. 2015, 49, 4226-4234

APPENDICES

Appendix A: X-Ray Diffractometry

Table A: Supplemental D-spacing values annotated in powder sample diffractogram of the muscovite sample *(Figure 1, Section 4.2)*

Table A: **Annotated d-spacing values in powder sample diffractogram**	
d-Spacing value (Å)	**Mineral**
9.96418	Muscovite
7.15977	Kaolinite
4.98793	Muscovite
4.45724	Muscovite, Kaolinite
4.29447	Muscovite, Quartz
4.10598	Muscovite
3.87449	Muscovite
3.73530	Muscovite
3.57812	Kaolinite
3.49122	Muscovite
3.32656	Muscovite, Quartz
3.20101	K-spar?
2.99227	Muscovite
2.86098	Muscovite
2.78960	Muscovite
2.59328	Muscovite, Kaolinite
2.50367	Muscovite, Kaolinite
2.49624	Muscovite
2.45878	Muscovite, Quartz
2.38058	Muscovite, Kaolinite
2.24549	Muscovite, Quartz
2.20396	Muscovite, Kaolinite
2.14984	Muscovite
2.13024	Muscovite, Quartz
2.05921	Muscovite
1.99669	Muscovite, Kaolinite, Quartz
1.96639	Muscovite
1.94612	Muscovite
1.81721	Muscovite, Quartz
1.78794	Kaolinite
1.73014	Muscovite
1.66131	Muscovite, Kaolinite
1.64507	Muscovite
1.59961	Muscovite

1.55670	Muscovite, Kaolinite, Quartz

Table B: D-spacing values annotated in air dried random oriented clay mount diffractogram *(Figure 2, Section 4.2)*

***Table B:* Annotated d-spacing values in air dried random oriented clay mount diffractogram**	
d-Spacing value (Å)	Mineral
9.99884	Muscovite
7.17005	Kaolinite
4.99852	Muscovite
3.58014	Kaolinite
3.33013	Muscovite, Quartz
3.19978	Muscovite
2.99527	Muscovite
2.86550	Muscovite
2.79476	Muscovite
2.56677	Muscovite, Kaolinite
2.49701	Muscovite
2.38636	Muscovite, Kaolinite

Table C (below): D-spacing values annotated in ethylene glycol solvated random orientated clay mount diffractogram *(Figure 3, Section 4.2)*

***Table C:* Annotated d-spacing values in glycol solvated random oriented clay mount diffractogram**	
d-Spacing value (Å)	Mineral
9.98465	Muscovite
7.15231	Kaolinite
4.99394	Muscovite
3.57931	Kaolinite
3.32983	Muscovite
3.19918	Muscovite
2.99268	Muscovite
2.79379	Muscovite
2.56987	Muscovite, Kaolinite
2.49952	Muscovite, Kaolinite
2.3879	Muscovite, Kaolinite

Appendix B: Major and Trace Element Analyses by Activation Laboratories, Ltd

The following is the full Certificate of Analysis, tabulation of results, and quality control information provided by Activation Laboratories, Ltd., after analysis of the muscovite test portion:

Quality Analysis ... Actlabs *Innovative Technologies*

Date Submitted: 16-Jan-17
Invoice No.: A17-00376
Invoice Date: 26-Jan-17
Your Reference:

Crawford Elliott
3278 Kensington Road
Avondale Est GA 30002
United States

ATTN: Crawford Elliott

CERTIFICATE OF ANALYSIS

1 Pulp samples were submitted for analysis.

The following analytical package(s) were requested: Code 8-REE Assay Package Major Elements Fusion ICP(WRA)/Trace Elements Fusion ICP/MS(WRA4B2)

REPORT **A17-00376**

Notes:

Total includes all elements in % oxide to the left of total.

CERTIFIED BY:

Emmanuel Eseme , Ph.D.
Quality Control

ACTIVATION LABORATORIES LTD.
41 Bittern Street, Ancaster, Ontario, Canada, L9G 4V5
TELEPHONE +905 648-9611 or +1.888.228.5227 FAX +1.905.648.9613
E-MAIL Ancaster@actlabs.com ACTLABS GROUP WEBSITE www.actlabs.com

Results **Activation Laboratories Ltd.** **Report: A17-00376**

Analyte Symbol	SiO2	Al2O3	Fe2O3(T)	MnO	MgO	CaO	Na2O	K2O	TiO2	P2O5	LOI	Total	Sc	Be	V	Cr	Co	Ni	Cu	Zn	Ga	Ge	As
Unit Symbol	%	%	%	%	%	%	%	%	%	%	%	%	ppm	ppm	ppm	ppm	ppm	ppm	ppm	ppm	ppm	ppm	ppm
Lower Limit	0.01	0.01	0.01	0.001	0.01	0.01	0.01	0.01	0.001	0.01		0.01	1	1	5	20	1	20	10	30	1	1	5
Method Code	FUS-ICP	FUS-ICP	FUS-ICP	FUS-ICP	FUS-ICP	FUS-ICP	FUS-ICP	FUS-ICP	FUS-ICP	FUS-ICP	FUS-ICP	FUS-ICP	FUS-ICP	FUS-ICP	FUS-ICP	FUS-MS	FUS-MS	FUS-MS	FUS-MS	FUS-MS	FUS-MS	FUS-MS	FUS-MS
Avant mica	46.78	34.24	1.57	0.014	0.55	0.02	0.52	7.51	0.883	0.03	7.11	99.24	39	3	176	90	3	< 20	10	30	58	1	< 5

Results **Activation Laboratories Ltd.** **Report: A17-00376**

Analyte Symbol	Rb	Sr	Y	Zr	Nb	Mo	Ag	In	Sn	Sb	Cs	Ba	Bi	La	Ce	Pr	Nd	Sm	Eu	Gd	Tb	Dy	Ho
Unit Symbol	ppm	ppm	ppm	ppm	ppm	ppm	ppm	ppm	ppm	ppm	ppm	ppm	ppm	ppm	ppm	ppm	ppm	ppm	ppm	ppm	ppm	ppm	ppm
Lower Limit	2	2	2	4	1	2	0.5	0.2	1	0.5	0.5	3	0.4	0.1	0.1	0.05	0.1	0.1	0.05	0.1	0.1	0.1	0.1
Method Code	FUS-MS	FUS-ICP	FUS-ICP	FUS-ICP	FUS-MS	FUS-MS	FUS-MS	FUS-MS	FUS-MS	FUS-MS	FUS-MS	FUS-ICP	FUS-MS	FUS-MS	FUS-MS	FUS-MS	FUS-MS	FUS-MS	FUS-MS	FUS-MS	FUS-MS	FUS-MS	FUS-MS
Avant mica	245	52	15	314	27	< 2	0.8	0.2	10	1.6	3.0	1444	< 0.4	7.6	15.3	1.69	6.5	1.3	0.55	1.7	0.4	2.5	0.6

Results **Activation Laboratories Ltd.** **Report: A17-00376**

Analyte Symbol	Er	Tm	Yb	Lu	Hf	Ta	W	Tl	Pb	Th	U
Unit Symbol	ppm	ppm	ppm	ppm	ppm	ppm	ppm	ppm	ppm	ppm	ppm
Lower Limit	0.1	0.05	0.1	0.04	0.2	0.1	1	0.1	5	0.1	0.1
Method Code	FUS-MS	FUS-MS	FUS-MS	FUS-MS	FUS-MS	FUS-MS	FUS-MS	FUS-MS	FUS-MS	FUS-MS	FUS-MS
Avant mica	1.8	0.29	2.0	0.31	7.9	2.3	6	0.8	14	3.1	1.7

QC **Activation Laboratories Ltd.** **Report: A17-00376**

Analyte Symbol	SiO2	Al2O3	Fe2O3(T)	MnO	MgO	CaO	Na2O	K2O	TiO2	P2O5	LOI	Total	Sc	Be	V	Cr	Co	Ni	Cu	Zn	Ga	Ge	As
Unit Symbol	%	%	%	%	%	%	%	%	%	%	%	%	ppm	ppm	ppm	ppm	ppm	ppm	ppm	ppm	ppm	ppm	ppm
Lower Limit	0.01	0.01	0.01	0.001	0.01	0.01	0.01	0.01	0.001	0.01		0.01	1	1	5	20	1	20	10	30	1	1	5
Method Code	FUS-ICP	FUS-ICP	FUS-ICP	FUS-ICP	FUS-ICP	FUS-ICP	FUS-ICP	FUS-ICP	FUS-ICP	FUS-ICP	FUS-ICP	FUS-ICP	FUS-ICP	FUS-ICP	FUS-ICP	FUS-MS	FUS-MS	FUS-MS	FUS-MS	FUS-MS	FUS-MS	FUS-MS	FUS-MS
NIST 694 Meas	11.50	1.88	0.74	0.013	0.34	42.90	0.88	0.54	0.117	30.15					1614								
NIST 694 Cert	11.2	1.80	0.790	0.0116	0.330	43.6	0.860	0.510	0.110	30.2					1740								
DNC-1 Meas	46.77	17.79	9.51	0.145	9.95	11.38	1.87	0.21	0.479	0.08			31		153	280	58	250	100	70	15		
DNC-1 Cert	47.15	18.34	9.97	0.150	10.13	11.49	1.890	0.234	0.480	0.070			31		148	270	57	247	100	70	15		
GBW 07113 Meas	71.53	12.85	3.20	0.143	0.15	0.60	2.49	5.44	0.282	0.05			5	4	< 5								
GBW 07113 Cert	72.8	13.0	3.21	0.140	0.160	0.590	2.57	5.43	0.300	0.0500			5.00	4.00	5.00								
LKSD-3 Meas																90	31	50	30	150			26
LKSD-3 Cert																87.0	30.0	47.0	35.0	152			27.0
W-2a Meas	52.49	15.28	10.61	0.165	6.25	11.01	2.21	0.61	1.080	0.15			35	< 1	272	100	43	70	110	80	18	1	
W-2a Cert	52.4	15.4	10.7	0.163	6.37	10.9	2.14	0.626	1.06	0.130			36.0	1.30	262	92.0	43.0	70.0	110	80.0	17.0	1.00	
SY-4 Meas	50.14	20.71	6.20	0.106	0.52	8.15	6.99	1.67	0.292	0.15			2	3	7								
SY-4 Cert	49.9	20.69	6.21	0.108	0.54	8.05	7.10	1.66	0.287	0.131			1.1	2.6	8.0								
CTA-AC-1 Meas																			60	40			
CTA-AC-1 Cert																			54.0	38.0			
BIR-1a Meas	47.85	15.74	11.15	0.172	9.56	13.47	1.80	0.02	0.971	0.03			44	< 1	313	380	53	180	130	80	16		
BIR-1a Cert	47.96	15.50	11.30	0.175	9.700	13.30	1.82	0.030	0.96	0.021			44	0.58	310	370	52	170	125	70	16		
NCS DC86312 Meas																							
NCS DC86312 Cert																							
NCS DC70009 (GBW07241) Meas																			990	100	17	11	63
NCS DC70009 (GBW07241) Cert																			960	100	16.5	11.2	69.9
OREAS 100a (Fusion) Meas																	17		180				
OREAS 100a (Fusion) Cert																	18.1		169				
OREAS 101a (Fusion) Meas																	48		440				
OREAS 101a (Fusion) Cert																	48.8		434				
JR-1 Meas																		< 20		30	17	2	17
JR-1 Cert																		1.67		30.6	16.1	1.88	16.3
NCS DC86318 Meas																							
NCS DC86318 Cert																							
Avant mica Orig	46.59	33.90	1.57	0.014	0.55	0.04	0.52	7.47	0.879	0.03	7.11	98.67	38	3	175	100	3	< 20	10	30	58	1	< 5
Avant mica Dup	46.97	34.59	1.57	0.013	0.56	0.01	0.51	7.55	0.887	0.03	7.11	99.81	39	3	178	90	3	< 20	10	30	58	1	< 5
Method Blank	< 0.01	< 0.01	0.02	0.002	< 0.01	< 0.01	< 0.01	< 0.01	0.001	< 0.01			< 1	< 1	< 5	< 20	< 1	< 20	< 10	< 30	< 1	< 1	< 5

QC **Activation Laboratories Ltd.** **Report: A17-00376**

Analyte Symbol	Rb	Sr	Y	Zr	Nb	Mo	Ag	In	Sn	Sb	Cs	Ba	Bi	La	Ce	Pr	Nd	Sm	Eu	Gd	Tb	Dy	Ho
Unit Symbol	ppm	ppm	ppm	ppm	ppm	ppm	ppm	ppm	ppm	ppm	ppm	ppm	ppm	ppm	ppm	ppm	ppm	ppm	ppm	ppm	ppm	ppm	ppm
Lower Limit	2	2	2	4	1	2	0.5	0.2	1	0.5	0.5	3	0.4	0.1	0.1	0.05	0.1	0.1	0.05	0.1	0.1	0.1	0.1
Method Code	FUS-MS	FUS-ICP	FUS-ICP	FUS-ICP	FUS-MS	FUS-MS	FUS-MS	FUS-MS	FUS-MS	FUS-MS	FUS-MS	FUS-ICP	FUS-MS	FUS-MS	FUS-MS	FUS-MS	FUS-MS	FUS-MS	FUS-MS	FUS-MS	FUS-MS	FUS-MS	FUS-MS
NIST 694 Meas																							
NIST 694 Cert																							
DNC-1 Meas		140	15	36						0.9		110		3.9			4.9		0.60				
DNC-1 Cert		144.0	18.0	38						0.96		118		3.6			5.20		0.59				
GBW 07113 Meas		41	44	408								499											
GBW 07113 Cert		43.0	43.0	403								506											
LKSD-3 Meas	75					< 2	2.0		2		2.4			48.9	94.2		44.6	8.0	1.50			5.0	
LKSD-3 Cert	78.0					2.00	2.70		3.00		2.30			52.0	90.0		44.0	8.00	1.50			4.90	
W-2a Meas	20	193	19	92	7	< 2					0.9	171	< 0.4	10.6	25.0		13.6	3.4	1.10		0.6	3.9	0.8
W-2a Cert	21.0	190	24.0	94.0	7.90	0.600					0.990	182	0.0300	10.0	23.0		13.0	3.30	1.00		0.630	3.60	0.760
SY-4 Meas		1214	116	537								351											
SY-4 Cert		1191	119	517								340											
CTA-AC-1 Meas														2200	3390		1170	166	46.9	133	14.6		
CTA-AC-1 Cert														2176	3326		1087	162	46.7	124	13.9		
BIR-1a Meas		107	14	18								7		0.7	2.0		2.6	1.1	0.53	1.9			
BIR-1a Cert		110	16	18								6		0.63	1.9		2.5	1.1	0.55	2.0			
NCS DC86312 Meas														2280	177		1600			240	31.3	185	35.1
NCS DC86312 Cert														2360	190		1600			225.0	34.6	183	36
NCS DC70009 (GBW07241) Meas	502						1.6	1.0	1660	3.4	42.0			23.9	61.1	8.00	32.4	12.7		16.1	3.1	22.0	4.3
NCS DC70009 (GBW07241) Cert	500						1.8	1.3	1701	3.1	41			23.7	60.3	7.9	32.9	12.5		14.8	3.3	20.7	4.5
OREAS 100a (Fusion) Meas						25								271	495	48.3	159	25.2	3.82	22.4	3.7	24.2	5.0
OREAS 100a (Fusion) Cert						24.1								260	463	47.1	152	23.6	3.71	23.6	3.80	23.2	4.81
OREAS 101a (Fusion) Meas						21								815	1380	130	402	49.6	8.37			32.3	6.5
OREAS 101a (Fusion) Cert						21.9								816	1396	134	403	48.8	8.06			33.3	6.46
JR-1 Meas	253				14	3		< 0.2	3		20.8		0.6	19.9	48.1	5.90	23.8	5.7	0.31		1.0	6.2	
JR-1 Cert	257				15.2	3.25		0.028	2.86		20.8		0.56	19.7	47.2	5.58	23.3	6.03	0.30		1.01	5.69	
NCS DC86318 Meas	392										11.1			1990	432	752	3290	1710	19.6	2300	505	3190	599
NCS DC86318 Cert	369.42										10.28			1960	430	740	3430	1720	18.91	2095	470	3220	560
Avant mica Orig	244	51	15	316	27	< 2	0.8	0.2	10	2.7	3.0	1441	< 0.4	7.4	15.1	1.70	6.7	1.3	0.54	1.6	0.3	2.5	0.6
Avant mica Dup	245	53	15	313	27	< 2	0.8	0.2	9	0.5	2.9	1446	< 0.4	7.8	15.4	1.68	6.3	1.4	0.56	1.7	0.4	2.6	0.6
Method Blank	< 2	< 2	< 2	< 4	< 1	< 2	< 0.5	< 0.2	< 1	< 0.5	< 0.5	< 3	< 0.4	< 0.1	< 0.1	< 0.05	< 0.1	< 0.1	< 0.05	< 0.1	< 0.1	< 0.1	< 0.1